Atomically-Resolved Studies of the Chemistry and Bonding at Silicon Surfaces

Robert J. Hamers* and Yajun Wang

Department of Chemistry, University of Wisconsin, 1101 University Avenue, Madison, Wisconsin 53706

Received November 8, 1995 (Revised Manuscript Received February 26, 1996)

Contents

I.	Introduction	1261
II.	Atomic-Level Studies of the Chemistry of Si(001)	1262
a.	Geometry and Electronic Structure of Clean Si(001)	1262
b.	Structure and Bonding of H on Si(001)	1263
c.	Interaction of Disilane (Si_2H_6) with Si(001)	1265
d.	Interaction of Halogens with Si(001)	1267
e.	Interaction of Oxygen with Si(001)	1269
f.	Interaction of Water with Si(001)	1270
g.	Interaction of Phosphine with Si(001)	1270
h.	Interaction of Ammonia with Si(001)	1273
i.	Interaction of Boron Hydrides with Si(001)	1273
j.	Interaction of Trimethylgallium with Si(001)	1276
k.	Interaction of Methyl Chloride with Si(001)	1277
l.	Interaction of Ethylene and Acetylene with Si(001)	1278
III.	Atomic-Level Studies of the Chemistry of Si(111)	1279
a.	Structure and Bonding of the Si(111)-(7×7) Surface	1279
b.	Interaction of H with Si(111)	1280
c.	Interaction of Silane with Si(111)	1281
d.	Interaction of GeH_4 and Ge_2H_6 with Si(111)-(7×7)	1283
e.	Interaction of Halogens with Si(111)	1283
f.	Interaction of Oxygen with Si(111)	1284
g.	Interaction of Ammonia with Si(111)	1285
h.	Interaction of Decaborane with Si(111)	1286
i.	Interaction of Acetylene with Si(111)-(7×7)	1287
IV.	Summary and Conclusions	1287

I. Introduction

Since the invention of the transistor in 1947, there has been a widespread and continuing interest in understanding the physical and chemical properties of semiconductor surfaces.[1] Despite the fact that the first transistor was made from germanium, over the last 47 years, silicon has received by far the lion's share of this attention, due largely in part to the presence of robust native oxide on silicon surfaces. Microelectronics remains one of the few areas of technology where it is essential to use single crystals of well-defined crystallographic orientation. Many of the rapid advances in microelectronics over the last 10 years, particularly since the advent of the personal computer, have been attained through a reduction in size. Common microprocessors for home use now use 0.35 μm technology. Continuing trends in microelectronics over the next 10−15 years will likely also require the ability to understand and control the surface chemistry of silicon and other semiconductors on length scales of <100 Å.

With the invention of the scanning tunneling microscope (STM) in the early 1980s,[2,3] it has now become possible to examine directly the structure and electronic properties of silicon (and other) surfaces with atomic resolution. Yet, the application of STM to problems of surface chemistry remains a challenging area. While the basic theoretical foundations of the STM imaging process are well understood in terms of the electronic states of the sample and the tip,[4−7] in practice one generally does not know a priori the distribution in energy or space of the electronic energy levels of most molecular fragments. Absolute chemical identification therefore can be obtained easily only in simple chemisorption systems whose electronic properties are well established. Yet, there remain other ways of gleaning chemical information from STM images. For silicon, the strong desire to achieve 4-fold coordination is providing routes to chemical identification based on direct observations of chemical coordination. Alternatively, electronic structure calculations can be performed for various structures, permitting a direct comparison with the scanning tunneling microscopy data. In some cases, chemical information can be obtained from counting statistics and the use of stoichiometric relationships. Perhaps the most important point is that the use of STM to investigate surface chemistry at an atomic level is yet in its infancy.

The interaction of foreign atoms or molecules with silicon surfaces typically involves an interplay between optimization of 4-fold coordination, pairing of electrons to achieve closed-shell configurations, and minimization of surface stress resulting from deviations from tetrahedral coordination. The following sections will review some of the investigations of the interaction of Si(001) with atomic or molecular species that are relevant for semiconductor microelectronics. Because of the enormous number of studies of silicon surfaces in their clean state and with a significant fraction of the elements in the periodic table, this review is selective and will focus primarily on those studies using scanning tunneling microscopy

* Author to whom correspondence should be addressed. Tel: 608-262-6371. Fax: 608-262-0453. E-mail: RJHAMERS@FACSTAFF.WISC.EDU.

S0009-2665(95)00213-5 CCC: $25.00 © 1996 American Chemical Society

Robert Hamers was born in Kenosha, WI, in 1958. He received a B.S. degree in chemistry from the University of Wisconsin-Madison in 1980 and a Ph.D. degree in physical chemistry from Cornell University in 1985. During his postdoctoral work at the IBM T. J. Watson Research Laboratory in Yorktown Heights, NY, he became one of the first researchers to achieve atomic resolution with the newly-invented scanning tunneling microscope. As a permanent research staff member at IBM from 1986 to 1990, he applied STM to investigate the structure, bonding, and reactivity of silicon surfaces and made significant contributions to the development of local tunneling spectroscopy techniques. In 1990, he joined the faculty at the University of Wisconsin-Madison, where he is Professor of Chemistry. His awards include the Peter Mark Memorial Award of the American Vacuum Society, a Presidential Faculty Fellowship from the National Science Foundation, and a Dreyfus New Faculty Award. Professor Hamers' research interests center on atomically-resolved studies of the chemical reactivity, geometry, and electronic properties of surfaces. Systems being investigated include semiconductors for microelectronics applications, molecular reactions during heterogeneous catalysis, and surface reactions of natural minerals.

Yajun Wang was born in Guanyun, People's Republic of China, in 1965. He received a B.Sc. degree in chemical physics from the University of Science and Technology of China, Hefei, People's Republic of China, in 1986. He then went to the Institute of Chemical Metallurgy of the Chinese Academy of Sciences, where he received a master's degree in chemical engineering in 1989. After he received a M.Sc. degree in chemistry from the University of Illinois at Chicago in 1992, he moved to the University of Wisconsin-Madison to pursue a Ph.D. degree in chemistry under the direction of Professor Robert J. Hamers. He is expecting a Ph.D. degree in May 1996. During his 4 years of graduate study in Professor Hamers' group, his research has focused on illustrating the atomic-level interaction between molecular precursors and silicon surfaces during chemical vapor deposition and doping processes using scanning tunneling microscopy and Fourier transform infrared spectroscopy.

to investigate the interaction of Si(001) and Si(111) surfaces with molecular species. An excellent recent review summarizing much of the chemistry of silicon surfaces can be found in ref 8.

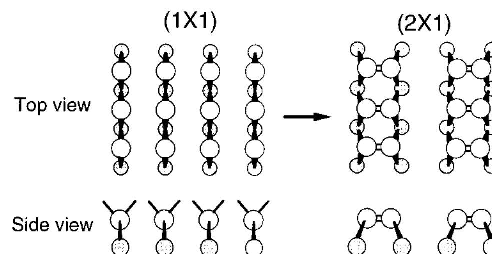

Figure 1. Structural model of Si(001), showing the surface (2×1) reconstruction.

II. Atomic-Level Studies of the Chemistry of Si(001)

a. Geometry and Electronic Structure of Clean Si(001)

The chemistry of the Si(001) surface is intimately connected with the geometry and electronic structure of the surface atoms. Much of the chemistry of this surface is driven by fact that Si is most stable with a coordination number of 4 in a tetrahedral geometry; however, this condition of stability is necessarily violated at a two-dimensional surface in the absence of foreign species. To understand the chemistry of Si(001), then, it is imperative to understand the nature of the Si(001) reconstruction. As shown in Figure 1, truncation of the bulk diamond structure along the (001) direction cuts through two Si−Si bonds for each Si atom. This leaves each Si surface atom with two bonds to the bulk and two "dangling bonds" with one electron in each. The surface reconstruction obtained by a simple lateral translation to form silicon dimers was first proposed by Schlier and Farnsworth in 1959.[9] While a number of alternative models were proposed,[10−12] electronic structure calculations have generally found that the dimer structure is the lowest in energy.[13−16] The Si(001) structure was finally confirmed on the basis of scanning tunneling microscopy results by Hamers and co-workers.[17−19]

Many properties of Si(001) can be understood on the basis of a simple picture of the bonding in the dimer.[13−16,20] For each pair of Si atoms, there are a total of four broken bonds; the rehybridization of these orbitals and concurrent motion of the Si atoms toward one another result in a Si dimer in which there is a strong σ bond linking the two atoms and a second weaker π bond. Thus, the Si surface dimers can be considered to have a double bond. Since STM images the surface electronic (not topographic) structure, it is possible to directly image the spatial distribution of the electronic states, particularly those that lie nearest the Fermi energy.[18,21] For example, Figure 2 shows STM images of the Si(001) surface imaging the occupied (a) and unoccupied (b) electronic states. The π molecular orbital has its maximum nearest the center of the Si=Si dimer bond, while the π^* antibonding orbital has a node in the wavefunction at this location. As a result, unoccupied state images of the π^* antibonding orbital show a deep minimum at the center of the Si=Si dimer bond as well as a minimum between the dimer rows.

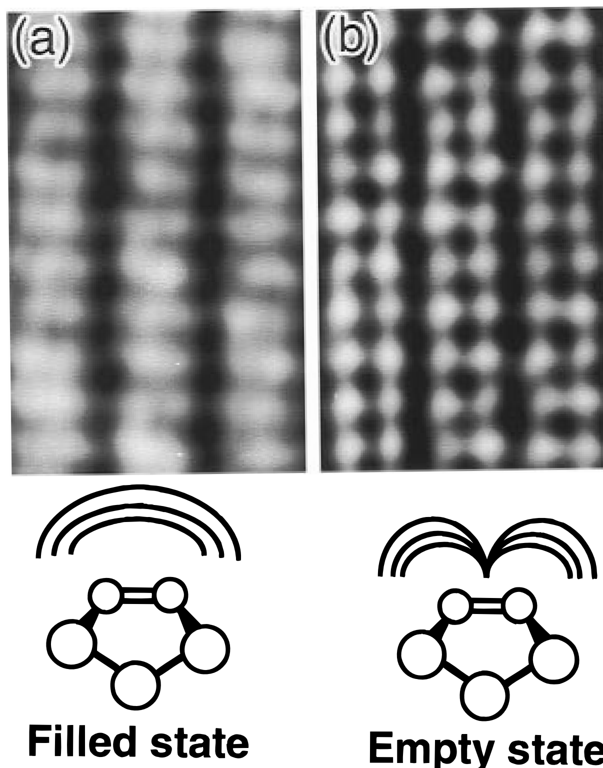

Figure 2. STM images of clean Si(001) surface probing the filled surface states and empty surface states: (a) $V_{\text{sample}} = -2.0$ V and (b) $V_{\text{sample}} = 2.3$ V. $I_{\text{tunnel}} = 0.2$ nA; dimensions = 23 Å × 77 Å.

While formally the silicon surface dimers have both a σ and a π bond, the π overlap of the Si surface dimers is poor; this occurs in part because the strained geometry at the surface prevents good spatial overlap of the orbital needed to achieve strong π bonding. The pairing energy associated with the dimer π bond on clean Si(001) has been estimated at values between 1 and 31 kJ/mol,[13,22−27] with most estimates clustering between 20 and 30 kJ/mol; this value is much smaller than the typical Si bond strength of 226 kJ/mol for bulk Si and 250−310 kcal/mol for silicon hydrides.[28,29] It is the weakness of this dimer bond and the fact that Si is most stable when tetrahedrally coordinated that control much of the reactivity of this surface.

Despite the apparent simplicity of the dimer model, there are some aspects of the Si(001) surface that remain unsolved. Even early studies of the Si(001) surface predicted that the surface should be more stable if the dimers tilt, so that the dimer axis is not parallel to the surface plane.[16] STM studies at room temperature have observed primarily nontilted dimers, while tilted dimers are typically visible near step edges or defects where the intrinsic symmetry is broken. When tilted dimers are observed, they always alternate from dimer to dimer along a row, giving rise to "zigzag" structures in the STM images. Correlation of the phase of this tilting between adjacent rows gives rise to c(4×2) symmetry or p(2×2) symmetry.[17−19] To reconcile the STM observations with electronic structure calculations, Hamers proposed that the appearance of symmetric dimers could result from dimers which were in fact tilted but flipping back and forth between the two equivalent tilt directions due to thermal excitation.[17]

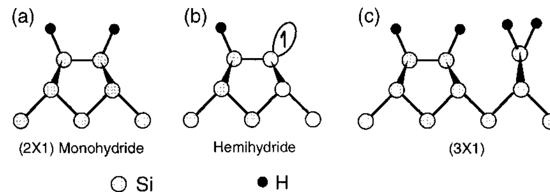

Figure 3. Structural model of hydrogen on Si(001), showing monohydride, hemihydride, and (3×1) structures.

Indeed, low-energy electron diffraction (LEED) studies as early as 1986[30] revealed a transition from (2×1) to c(4×2) symmetry, supporting this idea of dynamically-buckling dimers at 300 K. Recent studies at low temperature appear to confirm this picture: STM images at low temperature show Si(001) regions consisting primarily of dimers that are tilted in an alternating manner, producing a c(4×2) reconstruction.[31] At the present time the influence of dimer buckling on the chemical reactivity of Si(001) is not well understood. However, the tilting of a dimer has an associated charge transfer, in which electrons are transferred from the down atom to the "up" atom.[16,18] Thus, a tilted dimer presents to an impinging molecule a more electron-rich (nucleophilic) site than a dimer that is not tilted. Although the implications of this are yet unclear, it does appear that adsorption of strongly-electronegative and/or- electropositive adsorbates on the Si(001) surface tends to induce more dimer buckling than neutral adsorbates.[32]

b. Structure and Bonding of H on Si(001)

The simplest adsorbate is, of course, the hydrogen atom. The adsorption of hydrogen onto Si(001) has been one of the most heavily-studied systems in all of surface science.[33−39] This interest originates both in the fact that H on Si(001) is a model system for study and because of the important role that surface hydrogen plays in chemical vapor deposition processes in the microelectronics industry.[40,41] The interaction of Si(001) with molecular hydrogen is extremely weak with a reactive sticking probability of nearly zero;[37,42] this no doubt arises from the strength of the H_2 bond, which is far stronger than two Si−H bonds. In contrast, the reaction of Si(001) with atomic hydrogen (produced by thermal decomposition of H_2 on a hot tungsten filament or by decomposition of H-containing molecules on the surface) is facile, producing several possible ordered structures. The most heavily-studied structure is the monohydride. In the monohydride structure, each atom of Si has one attached H atom, as illustrated in Figure 3a, yielding a local coverage of one monolayer. At lower coverages it is possible to form a disordered "hemihydride" structure with a local coverage of one-half monolayer, as depicted in Figure 3b. In the hemihydride structure only one of the two Si atoms in a dimer is bonded to an H atom, while the other Si atom has a coordination number of 3, with one electron in a "dangling bond" orbital. At coverages of greater than one monolayer, it is possible to form an ordered (3×1) structure that consists of monohydride units alternating with SiH_2 groups, as in Figure 3c.[33]

The most commonly-studied H-induced Si(001) surface reconstruction is the monohydride structure,

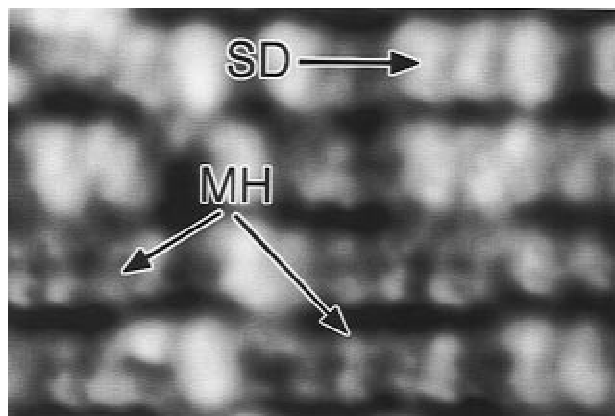

Figure 4. STM image showing clean and monohydride dimers on Si(001), prepared by thermal dissociation of disilane at 660 K. Area = 31 Å × 52 Å; V_{sample} = −3.0 V; I_{tunnel} = 0.5 nA (from refs 32 and 50).

in which H atoms bond to each end of the Si(001) dimer.[33−39,43,44] First identified in low-energy electron diffraction experiments in 1976,[33] this surface was first observed in STM after exposure of Si(001) to NH_3.[21,45] In this case, the NH_3 molecule dissociates, and the H atoms produced adsorb on nearby dimers and form the monohydride structure. More recent studies have shown the formation of the monohydride structure using atomic hydrogen (produced by the dissociation of H_2 on a hot tungsten filament)[46−49] or by the thermal dissociation of other hydrogen-containing molecules such as disilane.[32,50]

One of the most interesting features of H adsorption on Si(001) is the relative stability of the monohydride and hemihydride structures for H coverages of monolayer. STM images by Boland first showed that there was a strong tendency for H atoms to pair onto the same dimer even at low coverage.[47,48,51] This can be viewed as a disproportionation of the type 2Si−SiH → Si=Si + HSi−SiH. This disproportionation can be understood easily based on a simple understanding of the dimer bonding: The adsorption of H atoms onto two dimers requires breaking two dimer π bonds, while adsorption onto the same dimer requires breaking one bond only. Therefore, it should be thermodynamically favorable by approximately one dimer bond energy for H atoms to pair onto a single Si dimer. Although there is a large variation in the estimated value for this pairing energy (1−31 kJ/mol),[22−27] all calculations predict that H atoms are more stable when bonded onto a single dimer.

At moderate H concentrations, this preference for bonding onto a single dimer leads to a kind of chemical phase segregation at the dimer level. For example, Figure 4 shows occupied-state STM images of a Si(001) surface produced by exposing Si(001) to 0.6 langmuir of Si_2H_6 at 300 K and then annealing at 660 K for 5 min. Under appropriate STM biasing conditions, it is simple to discriminate between clean dimers and monohydride dimers.[46−48] Because bonding to hydrogen eliminates the π bond and because the newly-formed Si−H bonding and antibonding states lie far from the Fermi level, the Si atoms which are bonded to H appear dark while those that are not bonded to H appear bright. Additionally, the Si−H-filled electronic states are centered around the Si−H bonds rather than between the Si atoms, so that STM images of monohydride dimers show two protrusions within each unit cell, while clean Si=Si dimers appear as a single bean-shaped structure. At larger bias voltages of ca. 3 V, filled state images are able to readily distinguish between clean Si dimers, monohydride dimers, and dimer vacancies based on these differences.[50] Figure 4 shows that the hydrogen is distributed on the surface to form almost entirely dimers of the "monohydride" structure or dimers of clean Si and reveals the different apparent shapes of monohydride and clean silicon dimers.

Because the monohydride structure achieves 4-fold coordination for all Si atoms, it is generally thought that this structure is passive with respect to most other molecular reactants. This chemical passivation and the dimer-level phase segregation of H atoms on Si(001) have important implications for understanding the chemistry of molecules such as SiH_4 and Si_2H_6 on Si(001). One important result is the observation by Boland[46] that the reaction of disilane does in fact occur with the monohydride surface, albeit at a slower rate than with the clean surface. The nonzero reactivity of the monohydride structure in turn implies that it should be possible to grow silicon by chemical vapor deposition (CVD) processes at very low temperatures, since thermal desorption of the H_2 product is not an absolute necessity for reaction to occur. Additionally, it is known that exposure of the Si(001)-(2×1)H monohydride structure to atomic H can cause desorption of H_2;[34,52] it is thought that this occurs though an Eley−Rideal type reaction mechanism, in which an impinging H atom directly abstracts an H atom from the surface, leaving behind a bare Si atom.[53] While Boland's work shows that the monohydride structure has a nonzero reactivity, the possibility of such an Eley−Rideal mechanism suggests that there will also be "holes" in a monohydride-base passivation layer. Both these effects will lead to increased reactivity of the surface, with obvious implications for understand CVD reactions at low temperature and also for the use of passivating H layers as "resists" during nanometer-scale lithography operations.[54,55]

At H coverages below this saturation regime, the dimer-level phase segregation of H has some implications for understanding the mechanisms of CVD reactions. As will be discussed below, the adsorption of these molecules is generally believed to require two immediately-adjacent sites.[56−59] If H atoms were to randomly distribute on the surface, then at moderate H coverages there would be very few surface sites where two immediately-adjacent surface sites were present. Because the H atoms prefer to phase segregate as they do, the surface structure even at high H coverage consists of large regions of monohydride, a small number of "hemihydride" dimers, and a larger number of "clean" dimers. Only the latter provides two immediately-adjacent reactive sites on the surface.

The pairing of H atoms on Si(001) dimers also has implications for understanding the unusual desorption of H_2 from Si(001).[34,35,60] In general, the rate of recombinative desorption via the reaction $H_{ads} + H_{ads} \rightarrow H_{2g}$ would be expected to depend on the square of the hydrogen coverage. Numerous temperature-

programmed desorption studies have shown that the desorption of H_2 from the Si(001) monohydride structure depends only linearly on the surface coverage; in temperature-programmed desorption experiments, this is revealed as a peak temperature which is independent of surface coverage.[34,35,61−63] The observed pairing of H onto the Si(001) dimers suggests that the unusual desorption behavior occurs because the surface diffusion and pairing of H atoms onto a dimer is fast compared with the rate-limiting step in the thermal desorption process. As a result, the H atoms are essentially in close proximity, and the rate of thermal desorption is limited by the rate at which the two H atoms, already paired onto a single dimer, can pass through to the desorption transition state.[47] Experimental measurements have also probed the dynamics of H_2 desorption and have shown that the H_2 which desorbs is rotationally cold, implying a symmetric transition state.[64,65] At the present time many aspects of the hydrogen desorption process remain controversial.[66]

While exposure of Si(001) to atomic hydrogen near 600 K leaves only the monohydride structure, at lower temperatures it is possible for higher hydrides to form on the surface. At temperatures below 375 K, both SiH_2 and SiH_3 species have been detected, leading to the conclusion that the "(1×1)" phase observed at high H exposures at $T < 375$ K results from a disordered mixture of monohydride, dihydride, and trihydride species.[67] At higher temperatures the trihydride species become unstable, but at temperatures of ca. 500 K an ordered (3×1) structure has also been observed.[33,68] Using STM, Boland[69] showed that this structure consists of an alternating array of SiH_2 groups and H−Si−Si−H monohydride dimers as depicted in Figure 3; the hydrogen coverage is therefore one and one-third monolayer.

c. Interaction of Disilane (Si_2H_6) with Si(001)

The interaction of disilane (Si_2H_6) with Si(001) has been widely studied as a model system for understanding CVD growth processes. Although silane (SiH_4) is the most common CVD precursor used in the microelectronics industry, Si_2H_6 is safer and has significantly higher reactivity. The reaction of disilane on Si(001) has been widely investigated using conventional surface science methods,[56−59,70−79] as well as scanning tunneling microscopy.[32,46,50,80−82]

While the thermal decomposition reactions of both silane and disilane are thermodynamically favorable (the free energies of formation are 56 and 127 kJ/mol, respectively),[83] the activation barriers to the initial bond breakage make their decomposition slow. In disilane, the weaker Si−Si bond (335 kJ/mol)[29] gives it higher reactivity than silane, which presumably interacts with Si(001) through cleavage of a Si−H bond (energy ca. 390 kJ/mol).[29] In the case of silane, reaction involves breaking a Si−H bond and the weak dimer π bond while forming new SiH_3−surface and H−surface bonds. In the case of disilane, reaction involves breaking the disilane Si−Si bond (335 kJ/mol) and the dimer π bond (20−30 kJ/mol) while forming two new $Si_{surface}$−SiH_{3ads} bonds (ca. 335 kJ/mol each). In both cases, a simple analysis of the energy balance suggests that dissociative adsorption is only favorable if both initial fragments of decomposition (either $2SiH_3$ groups or $SiH_{3ads} + H_{ads}$) remain bonded to the surface. Since Si−H bonds are stronger than Si−Si bonds, the possibility of continuous growth by decomposition of hydrides is a direct result of the fact that CVD reactors are open thermodynamic systems, as recombinative desorption of H_{ads} as H_{2g} permits the dissociation reactions to proceed continuously.

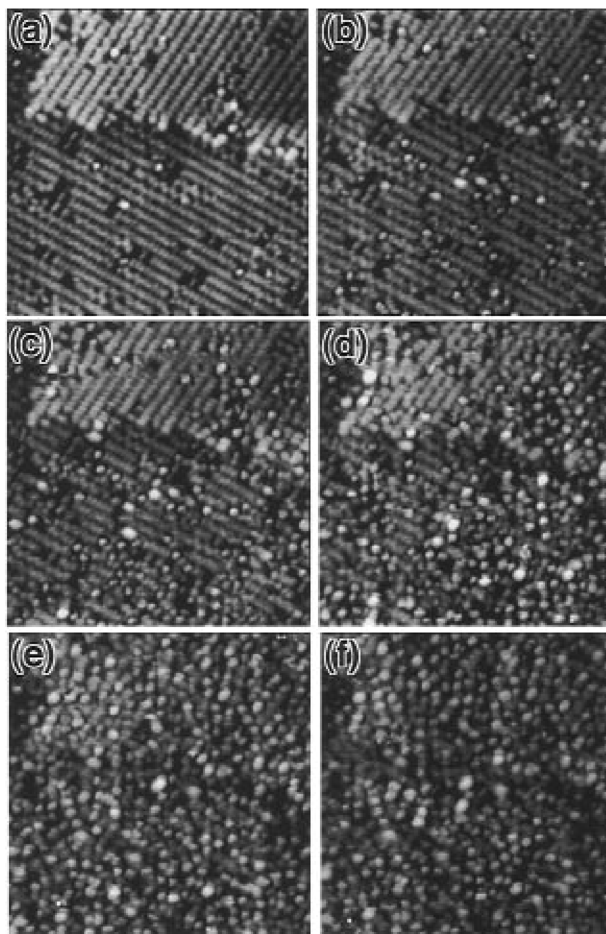

Figure 5. Sequential images of Si(001) obtained while simultaneously dosing with disilane at room temperature: (a) exposure of 0.1 langmuir; other images are taken 230 s apart. Surface area = 200 Å × 200 Å; $V_{sample} = -2.2$ V; $I_{tunnel} = 0.5$ nA (from ref 32).

Figure 5 shows a sequence of STM images of a single region of Si(001) surface during exposure to disilane at 300 K. The STM images show several important features. First, we note that the decomposition fragments are randomly distributed on the surface, with no significant increase near the atomic step; this implies that steps do not have a strong influence on the initial steps of the surface reaction. Second, we note that the adsorption of Si_2H_6 is believed to occur by cleavage of the Si−Si bond,[28,58] producing two adsorbed SiH_3 fragments for each incident Si_2H_6 molecule. Yet the STM images clearly show that there is no observable "pairing" of the fragments; this in turn indicates that the exothermicity of the initial reaction step $Si_2H_6 \rightarrow 2SiH_{3ads}$ is sufficient to randomize the spatial locations of the fragments.

In the decomposition of any molecular species such as disilane, a general difficulty that must be faced

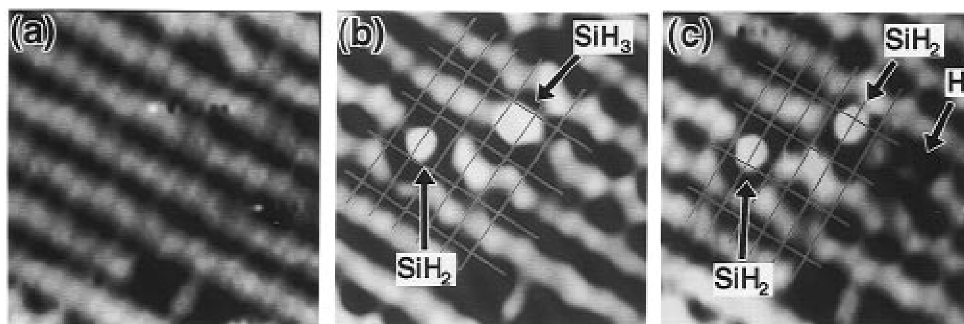

Figure 6. Sequential images of Si(001) surface showing adsorption of SiH_2 and SiH_3 and the dissociation reaction SiH_3(ads) → SiH_2(ads) + H(ads): (a) clean Si(001) surface before exposure to Si_2H_6, (b) same area as in part a after exposure to 0.1 langmuir of Si_2H_6 at 300 K, showing adsorbed SiH_2 group (left) and SiH_3 group (right), and (c) same region as in parts a and b, acquired 8 min after b, showing the shift in bonding location as SiH_3 group dissociates to SiH_2 and the appearance of atomic-sized depression due to H atom adsorption. Area = 47 Å × 47 Å; $V_{sample} = -2.2$ V; $I_{tunnel} = 0.5$ nA (from ref 32).

in the use of STM is the fact that although STM can distinguish between chemically-inequivalent fragments on a surface, actual identification of these fragments is more difficult. Bronikowski, Wang, and Hamers[32,80] showed that this could be accomplished using atomic-resolution images to establish the bonding locations of the fragments with respect to the underlying Si(001) lattice. Since the structure of the underlying Si(001) surface is well understood, a measurement of the location of a molecular fragment directly reveals its coordination number N. If it is assumed that all silicon-containing fragments will attempt to achieve 4-fold coordination for the Si atom, then the number of hydrogen atoms attached to any fragment is just $(4 - N)$.

To illustrate this coordination-based approach to chemical identification, Figure 6 shows a sequence of high-resolution STM images of a single region of the Si(001) surface. Figure 6a shows the clean starting surface, while Figure 6b shows the same region after exposure to 0.1 langmuir of Si_2H_6. Figure 6b shows that two fragments have entered the field of view; however, these two fragments are clearly different, distinguishable by their different apparent height, apparent shape, and local bonding symmetry. On the basis of the coordination arguments described above, we assign one fragment (at a bridge-bonded location) to an SiH_2 group and another fragment (at a terminal position with only one bond to the surface) to an SiH_3 group. Eight minutes later, the third panel (Figure 6c) shows that the fragment originally assigned to an SiH_3 group has clearly changed both its apparent height and its bonding location and now appears identical with the other fragment already assigned as an SiH_2 group. Note the appearance of a small dark depression; it is known from previous work (see section on H/Si(001) above) that the latter is the characteristic signature of a hydrogen atom. Thus, the sequence of images in Figure 6 shows the spontaneous dissociation of an SiH_3 group into an SiH_2 group plus an adsorbed H atom: $SiH_{3ads} \rightarrow SiH_{2ads} + H_{ads}$.

Using such methodology, Wang et al.[32] succeeded in identifying the SiH_3 and SiH_2 fragments produced by Si_2H_6 dissociation on Si(001). Further dissociation beyond SiH_2 is complicated by the fact that there is no simple way for an isolated "SiH_{ads}" fragment to bond on the Si(001) surface, since such a fragment would optimally have three bonds to the surface, while the Si(001) surface has rectangular symmetry. The apparent absence of a site where an adsorbed SiH fragment might form three bonds to the surface suggests that an SiH_{ads} fragment might not be a stable intermediate in the dissociation of Si_2H_6 and, if present at all, would be a high-energy intermediate. As shown in Figure 7, annealing the sample to induce further decomposition leads to an interesting result: A new form of surface dimer was observed, in which the axis of the newly-formed dimer was parallel to the dimer of the substrate (labeled "NRD"). In contrast, in normal epitaxial growth the dimers rotate by 90° between layers due to the overall tetrahedral coordination. In addition to these nonrotated dimers (NRD), two types of individual dimers were observed which are in the normal configuration for epitaxial growth. One type is directly atop the dimer row of the underlying substrate, while the second lies in the trough between dimer rows. Normal epitaxial growth involves alternating "A" and "T" dimers to form dimer rows. Figure 7 shows both STM images and the schematic geometry of the NRD, A, and T dimers.

How are these nonrotated dimers formed? Wang et al. found that up to 40% of the surface dimers could be nonrotated dimers (NRD's), suggesting that they play an important role in the decomposition mechanism. NRD's were also observed which appeared to have H atoms adsorbed on them (much as the presence of H on regular Si dimers changes their appearance). Wang et al. proposed that hydrided and clean NRD's might be a kinetic intermediate in the decomposition of the SiH_2 groups, providing a decomposition pathway without going through a discrete SiH(ads) moiety. It was noted that in temperature-programmed desorption measurements of Si_2H_6/Si(001), there are two desorption peaks: The β_1 peak arises from H_2 desorption from the monohydride phase, while the β_2 peak arises from desorption of H_2 from SiH_2 units, is second order in coverage, and accounts for one-third of the total hydrogen.[73] The proposed reaction mechanism is therefore that SiH_2 groups, which are mobile on the surface at elevated temperatures, diffuse until they become adjacent to one another. In this position the H atoms are in close proximity, and desorption of H_2(g) leaves behind a nonrotated dimer which is hydrogen-terminated. This

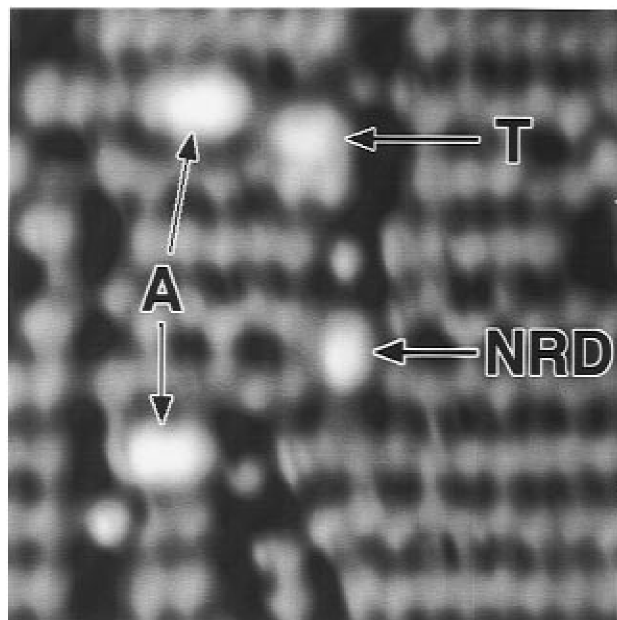

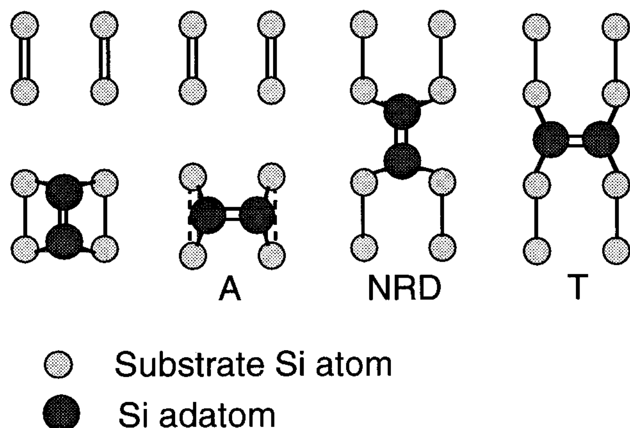

Figure 7. Atomic-resolution STM image and schematic model showing different dimer configurations observed during decomposition of Si_2H_6 on Si(001). STM image (top) taken after exposure to 0.2 langmuir of Si_2H_6 at 300 K and subsequent anneal at 470 K for 2 min, showing different bonding locations of three types of dimer structures. Area = 70 Å × 70 Å; $V_s = -2.0$ V; $I_t = 0.5$ nA. Bottom: model for four possible Si=Si ad-dimer structures which achieve 4-fold coordination for adsorbing silicon atoms. The structures shown in A, T, and NRD are found in the above figure (from ref 32).

can readily lose its hydrogen atoms to form a "normal" epitaxial dimer and continuous growth of the next Si layer. This mechanism, illustrated in Figure 8, appears to explain the atomic structure visible in the STM images and accounts for the relative intensities of the β_1 and β_2 peaks.

The decomposition of Si_2H_6 on Si(001) was also followed at higher hydrogen coverages by Boland.[46] As discussed in section IIb, at high hydrogen coverages the surface consists primarily of the Si(001)-(2×1)H monohydride structure, which is less reactive than the clean surface. However, Boland conducted STM investigations in which a Si(001)-(2×1)H monohydride surface was first prepared and then exposed to Si_2H_6 at 690 K.[46] The STM images showed that epitaxial growth occurred under these conditions, even though the surface was nominally saturated with hydrogen. A calculation of the rate of desorption

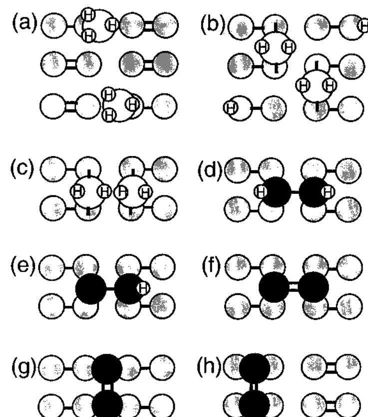

Figure 8. Model depicting the proposed mechanism for the decomposition of Si_2H_6 on Si(001) (from ref 32).

of H_2 at 690 K showed that the observed growth could not be accounted for simply by the presence of a small number of dangling bonds remaining on the surface, indicating that while the monohydride surface is certainly less reactive than the clean surface, it does exhibit at least some small reactivity toward Si_2H_6. Boland suggested that it might therefore be possible to grow thicker layers of Si using hydrogen to passivate the surface toward undesirable contaminants. This result is significant particularly for atomic-layer epitaxy processes,[79,84] for which a self-terminating surface chemical reaction is usually needed.

d. Interaction of Halogens with Si(001)

The interactions of halogens on Si(001) are important to semiconductor etching processes as well as deposition processing using common precursors such as SiH_2Cl_2. Like hydrogen, halogens require only one more electron to form a closed-shell configuration. As a result, they readily bond to the Si(001) surface, terminating the "dangling bonds" in much the same way that hydrogen does in the monohydride structure. One of the most interesting halogen systems has been chlorine on Si(001).[85-90] At high chlorine exposures, it is generally recognized the Cl_2 does indeed form a (2×1) "monochloride" structure at one monolayer Cl coverage.[86,88,90] Indeed, STM investigations using methyl chloride as a chlorine source show formation of ordered (2×1) monochloride regions.[91] While adsorption of molecular Cl_2 appears to saturate at one monolayer coverage, the interaction of Si(001) with atomic Cl appears to continue to at least one and one-half monolayer coverage; presumably the latter involves breaking of the backbonds between the surface Si dimers and the underlying substrate.

At low coverages, the bonding of chlorine with Si(001) is quite interesting. Surprisingly, an electron-stimulated desorption ion angular distribution (ESDIAD) investigation of this system by Cheng and co-workers revealed that the initial dissociative adsorption of Cl_2 onto Si(001) produced a single ESDIAD feature normal to the surface, while after annealing to 673 K the ESDIAD pattern irreversibly transformed into a four-beam pattern.[89] The normal peaked angular distribution produced upon initial adsorption was attributed to a bridge-bonded struc-

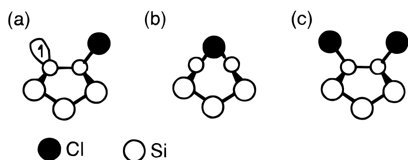

Figure 9. Model of Cl on Si(001) surface, showing different structures.

ture in which a Cl atom bonds to both Si atoms of a single dimer, while the structure observed after annealing was attributed to attachment of the Cl atom to the "dangling bond" at the end of the dimers, tilted 25° with respect to the surface normal. These two configurations are depicted schematically in Figure 9. A subsequent high-resolution electron energy loss spectroscopy (HREELS) investigation[88] also found evidence for two bonding locations for Cl on Si(001), consistent with the interpretation of Cheng. However, another ESDIAD study by Bennett and co-workers[87] found evidence for both normal and off-normal emission after 300 K exposure but reported only normal emission after annealing to 500 K; these observations are nearly the reverse of those of Cheng et al. Bennett et al.[87] interpreted the off-normal emission after 300 K exposure to dichloride species formed from two Cl atoms bonded to a single Si atom, and they attributed the normal emission to Cl atoms bonded at the dangling bond position of a strongly-tilted dimer.[87] It should also be noted that Bennett et al.[87] used an electrochemical chlorine source, while Cheng et al.[89] and Gao et al.[88] used molecular chlorine.

The presence of two possible bonding locations for Cl on Si(001) was confirmed in STM experiments by Boland.[92] While the stable bonding configuration appeared to be that which has Cl bonded to the dimer "dangling bond", a metastable bridge-bonded configuration was also observed. Moreover, Boland found that it was possible to force the Cl atoms to convert from one configuration to the other by applying an appropriate voltage between sample and tip. Under some conditions, the Cl atom appeared to be continuously shifting between the two equivalent dangling bonds of a single dimer, while at other times it appeared to form a symmetric doublet structure. Boland interpreted the symmetric doublet structure to the bridge-bonded chlorine proposed earlier by Cheng.[89]

While the work of Boland appears to support the interpretation of Cheng et al.[89] and Gao et al.,[88] there are still some unresolved questions for this system. One unresolved issue is understanding the differences in reactivity and the resulting surface structures between molecular chlorine and atomic chlorine. Another unresolved question regarding this structure is whether the Cl is bonded to both Si atoms through their π orbitals, or whether the stronger dimer σ bond is broken.

Like chlorine and hydrogen, bromine can also form a (2$\times$1) structure in which Br atoms terminate the dangling bonds of the Si(001) structure, giving rise to a (2$\times$1) reconstruction.[93–95] It again appears that the pairing of two Br atoms onto a single dimer is favorable, so that dimers with only a single Br adatom are observed only rarely.[95] As the total

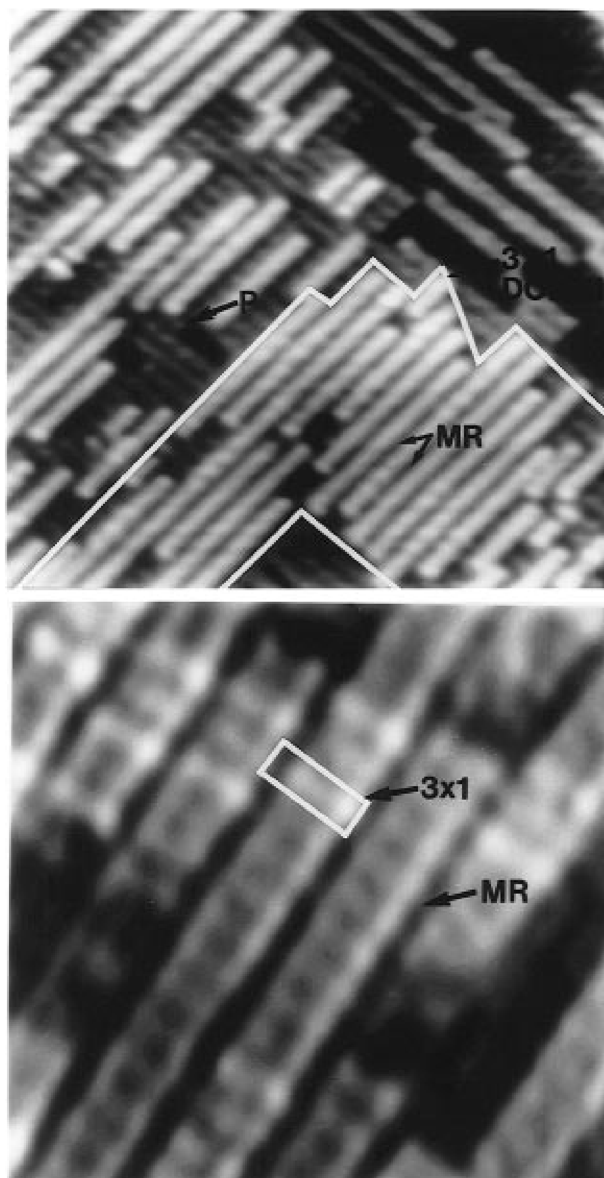

Figure 10. (top) Occupied-state image of Si(001) after 2.4 mAs Br exposure at 900 K (230 Å × 230 Å, −1.8 V, 0.05 nA) where patterning dominates. (bottom) Smaller scale image where the (3×1) unit cell of the missing row structure is outlined (from ref 95).

surface Br coverage increased toward one monolayer at 300 K, Rioux et al. noted the number of vacancy defects increased significantly. They proposed that at high exposures, an impinging Br_2 molecule which encounters a Br-terminated Si atom might form volatile $SiBr_3$ species; the desorption of these species into the gas phase would leave the surface with an apparent increase in vacancy defects. At elevated temperatures, the long-range correlations lead to the possibility of a (3$\times$1) structure in which Si_2Br_2 "monobromide" dimers alternate with $SiBr_2$ units, analogous to the (3$\times$1) reconstruction of H-terminated Si(001). While in the hydrogen case the SiH_2 units are stable, the $SiBr_2$ units are apparently volatile at temperatures >850 K. The net result of this volatility is that exposure of Si(001) to Br_2 at temperatures between 850 and 900 K leads to the formation of a new (3$\times$1) phase, in which Si_2Br_2 "monobromide" dimers alternate with vacancies. STM images[95] of the (3$\times$1) structure are shown in Figure 10, while

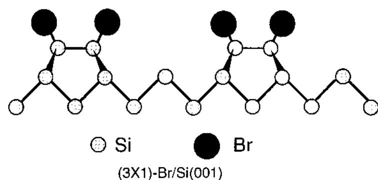

Figure 11. Structural model for the (3×1) structure of Br on Si(001).

Figure 11 shows the schematic structure of the (3×1) phase. This structure presumably results from the transient formation of a (3×1) phase containing $SiBr_2$ units followed by rapid desorption of $SiBr_2$ into the gas phase. At temperatures >900 K, the (3×1) structure was not observed; because the rate of Br_2 desorption from the monobromide phase is rapid at this temperature, the possibility of forming $SiBr_x$ species with $x > 1$ is significantly reduced, and the (3×1) structure cannot form at the fluxes used in the experiments.

The above discussion shows many similarities in the behavior of hydrogen, Cl, and Br on the Si(001) surface. These strong similarities arise from the fact that each of these species requires only one more electron to achieve a complete coordination sphere; as a result, forming a single bond at the "dangling bond" position of the Si(001) dimer permits these species to achieve complete coordination for the small cost of a dimer π-bond energy. Likewise, the fact that Si−H, Si−Cl, and Si−Br bonds are all stronger than Si−Si bonds results in the possibility of etching via the sequential formation of SiX_2, SiX_3, and, ultimately, volatile SiX_4 species. These reactions are thermodynamically favorable but are kinetically unfavorable under most circumstances. In contrast, the reaction of oxygen with Si(001) does not form nicely-ordered structures because oxygen, demanding a coordination number of 2, cannot easily achieve "ideal" coordination through formation of a simple adlayer but instead requires breaking of the backbonds between the dimers and the underlying substrate.

e. Interaction of Oxygen with Si(001)

One of the most important reactions in semiconductor microelectronics is the oxidation of Si(001).[96−101] Interfacial defects at the Si−SiO_2 interface play a very important role in properties of metal oxide semiconductor field effect transistors (MOSFETs). It has long been known that the trapping of electrons at the Si−SiO_2 interface represents a major component of the noise in small-area MOSFETs.[102,103] The continuing shrinkage of semiconductor devices also places new demands on the ability to grow ultrathin oxides, as applied field strengths approach breakdown values.

Early studies of the oxidation of Si(001) by Koch and Hamers[104,105] showed that exposure of Si(001) to oxygen produced surfaces with a patchy appearance. The oxidized regions appeared lower than the underlying surface due to the fact that oxidation reduces the density of electronic states near the Fermi energy. In the course of scanning the tip over these oxidized regions, it was shown that the tunneling current would often show a bistable behavior. This bistable behavior was attributed to the trapping of electrons in the interface states produced by Si oxidation. By analyzing the temporal distribution of the trap switching noise, it was possible to extract activation energies for trapping and detrapping electrons in individual trap states.

Experiments of the very initial stages of oxidation show it to be rather complicated. Molecular beam scattering studies have shown that the sticking coefficient of O_2 on Si(001) is small and decreases from 0.02 to 0.004 as the surface temperature is increased from 120 to 600 K.[106,107] Such behavior is typical of adsorption mediated by a molecular precursor state. There is also evidence that defects, particularly the "C"-type defects which are frequently observed on Si(001),[108] are facile sites for oxidation.[100,109] Cahill and Avouris[99,100] found that after exposing Si(001) to O_2 at 300 K, the originally flat surface was decorated with small amounts of silicon which formed small rows of dimers. A comparison of filled- and empty-state images confirmed that the ejected material consisted of silicon which was apparently ejected from the substrate due to the exothermicity of the Si oxidation reaction. The enthalpy of formation of SiO_2 (from crystalline Si and O_2) is −850 kJ/mol or 8.8 eV, compared with the Si−Si bond strength in bulk Si of only 226 kJ/mol.[28,29] Thus, it is perhaps not surprising that the large amount of energy release in the form of heat is sufficient to eject material onto the surface plane. The ejection of material might also be aided by the fact that the insertion of SiO into a Si−Si bond is likely to produce a significant amount of strain due to the different molar volumes of Si and SiO_2. Cahill and Avouris noted that the thermal ejection of Si onto the terrace might also be related to the formation of self-interstitials in Si during oxidation; such interstitials may play a role in dopant diffusion in bulk Si.[110,111] Unfortunately, STM studies of Si(001) have not been able to identify the locations of the oxygen atoms. EXAFS studies, however, have suggested that oxygen is present in two types of bridge sites: one in which the oxygen lies between Si atoms in the topmost layer and another in which the oxygen bonds between Si atoms of the first and second layers.[112]

On a larger scale, the structure of SiO_2 thin films and the desorption of SiO from the Si(001) surface has been investigated using a variety of techniques. Using scanning electron microscopy, Liehr and coworkers[113,114] showed that the decomposition of SiO_2 films of 50−500 Å thickness occurred heterogeneously, forming circular voids on the surface. Later studies using electron microscopy and temperature-programmed desorption experiments showed that this heterogeneous desorption process also occurred for thinner films.[115−117] Recent scanning tunneling microscopy investigations by Johnson and co-workers[101,118] have directly resolved the formation of circular voids with nearly atomic resolution. A quantitative analysis of the void areas as a function of the fraction of the SiO_2 desorbed showed that the rate of desorption scaled as $A^{1.0}$, where A is the island area. The significance of this observation is revealed through a simple analysis of the kinetics. Johnson

and Engel proposed the following overall mechanism for desorption of SiO from Si(001):

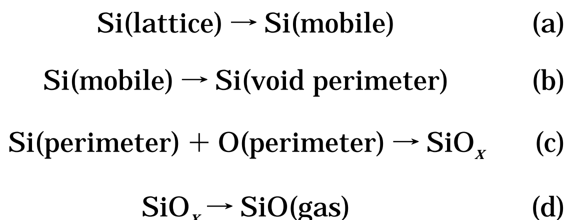

$$\mathrm{Si(lattice)} \rightarrow \mathrm{Si(mobile)} \quad \text{(a)}$$

$$\mathrm{Si(mobile)} \rightarrow \mathrm{Si(void\ perimeter)} \quad \text{(b)}$$

$$\mathrm{Si(perimeter)} + \mathrm{O(perimeter)} \rightarrow \mathrm{SiO}_x \quad \text{(c)}$$

$$\mathrm{SiO}_x \rightarrow \mathrm{SiO(gas)} \quad \text{(d)}$$

If decomposition at the void edge (eq d) is rate-limiting, then the rate would be expected to scale as $A^{0.5}$. Since Si diffusion is known to be fast with an activation barrier of only 70 kJ/mol (0.75 eV), step b can be ruled out. However, the first step (a), which represents the formation of a mobile adatom from Si on a terrace site, is expected to have a large activation barrier. The experimental values of the activation barrier for SiO desorption are ca. 340−375 kJ/mol[115,116] (3.5−3.9 eV) and appear to be independent of the oxide layer thickness; these values are in agreement with the calculated values for the activation barrier for creating a mobile monomer[119,120] and appear to support this kinetic analysis.

f. Interaction of Water with Si(001)

The interaction of water with Si(001) is of great technological importance in the "wet" oxidation of silicon.[121−123] An additional important result of the STM studies is that they show that many of the defects commonly observed on Si(001) can be attributed to molecularly-adsorbed water. Andersohn and Kohler[124] and Chander et al.[125] independently investigated this system, with many common results. At high coverage, spectroscopic measurements show that at least some water dissociates, producing Si−H and Si−OH species.[126−128] Because the (2×1) surface structure is preserved, it is thought that these species terminate the dimer dangling bonds, leaving the dimer σ bond intact.

At low coverage, both Chander et al.[125] and Andersohn et al.[124] reported that the interaction of H_2O with Si(001) eliminated dangling bonds in pairs. Chander et al. proposed that the water molecules are undissociated. They classified the observed water-induced features into different types. Type "M" features appear identical with the "missing dimer" defects commonly observed on Si(001), which appear identical with a simple dimer vacancy. Type "W" features appear as a set of two bright protrusions located on the same side of two adjacent dimers, with the other end of each dimer appearing as a depression. These type "W" features appear identical with the type "C" defects previously identified by Hamers and Kohler.[108] Through careful studies as a function of water exposure, it was found that the "W" and "M" features both increased in proportion to the water exposure. Because these defects appear identical in every way with the previously-identified missing dimer defects and "C"-type defects, it appears that they have the same origin and that therefore the missing dimer defects and "C"-type defects are not intrinsic to the Si(001) surface. Chander et al. proposed a bonding configuration like that shown in

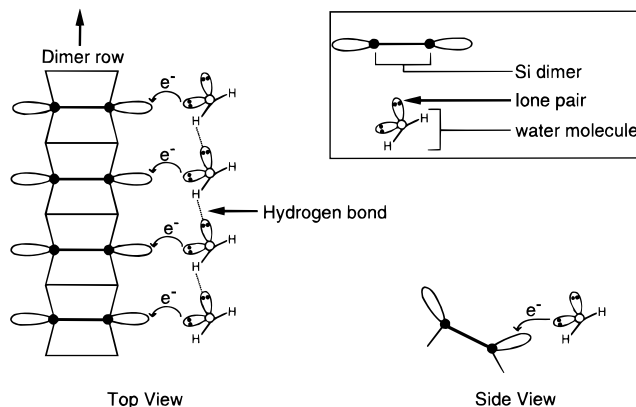

Figure 12. Proposed bonding geometries for H_2O/Si(001) and formation of "C"-type defects (from ref 125).

Figure 12: It involves a transfer of electrons from the oxygen lone pair to the "down" atom of a tilted dimer (which is electron-poor) and hydrogen bonding between adjacent water molecules. The "C"-type defect is believed to arise from two water molecules which are hydrogen-bonded in this way. At higher exposures water molecules can cluster together to form larger chains of this same type.

g. Interaction of Phosphine with Si(001)

1. Adsorption, Dissociation, and Surface Structure for Phosphine/Si(001)

Phosphine (PH_3) is a common precursor used for introducing phosphorus as an n-type dopant in silicon and is used in the heteroepitaxial growth of GaP on Si(001). Early studies showed that PH_3 tends to decrease the rate of Si growth.[129−131] The recent invention of "surfactant" growth techniques,[132,133] in which a group V element such as As or Sb is used to passivate the Si surface during growth to permit metastable growth of materials such as Ge on Si, has mandated a better understanding of the behavior of As, Sb, and P on Si(001).

In the earliest investigation of PH_3 interacting with Si(001), Yu and Meyerson observed an ordered (2×1) LEED pattern after PH_3 exposure and concluded that PH_3 adsorbed molecularly.[134,135] They proposed that the PH_3 molecule bonded in a vertical orientation, with the lone pair electrons of the phosphorus atom interacting with the Si═Si dimer bond electrons. Using electron energy loss spectroscopy, Colaianni et al.[136] showed that the interaction of PH_3 with Si(001) was at least partially dissociative, as a distinctive PH_2 scissor mode vibration was observed at 1050 cm^{-1}. Wang et al. investigated the interaction of phosphine with Si(001) at room temperature and at elevated temperatures using both STM[137,138] and infrared spectroscopy.[77,139] Scanning tunneling microscopy images of Si(001) exposed to PH_3(ads) showed localized domains of c(4×2) symmetry which were attributed to molecularly-adsorbed PH_3;[137] since the domain size was small, the presence of several domains of ordered c(4×2) symmetry would be expected to give rise to a LEED pattern with an apparent (2×1) symmetry, in agreement with the earlier observation of Yu and Meyerson.[131,134] Subsequent infrared spectroscopy by Shan et al.[139] con-

firmed that PH_3 can adsorb molecularly on Si(001), giving rise to a set of three peaks with frequencies nearly identical with those observed for PH_3 adsorbed molecularly on Si(111). In addition, however, on Si(001) additional peaks attributed to PH_{2ads} and H_{ads} were observed; this indicates that adsorption is at least partially dissociative, in agreement with the results of Colaianni et al.[136] Shan[139] showed that the extent of dissociation could be controlled by changing the rate of exposure, with rapid saturation at $P = 10^{-6}$ Torr giving rise to almost completely molecular adsorption but slow exposure at 5×10^{-9} Torr producing more extensive dissociation.

The bonding of molecular PH_3 to Si(001) is quite interesting because it involves a dative bond of the phosphorus lone pair orbitals. It is well known that tilting of the Si(001) dimers transfers electrons from the "down" atom to the "up" atom.[16,18] The "down" atom thereby becomes depleted of electrons and can accept additional electrons from the lone pair of PH_3. Ab initio theoretical calculations of PH_3 on Si(001) indeed show that the PH_3 bonds to the "down" atom of a tilted dimer with a binding energy of 96 kJ/mol (1.0 eV).[139,140] STM images show that even at low coverage some ordering of the PH_3 molecules occurs, with PH_3 molecules bonding at every second site along the dimer rows but with poorer correlation between dimer rows.[137] Since tilted dimers always alternate the direction of tilting, it is thought that the correlated bonding within one dimer row results from the fact that once one PH_3 molecule bonds and produces a tilted dimer−PH_3 adsorption site, nearby dimers also tilt in an alternating configuration; this in turn forms electrophilic and nucleophilic sites that likely result in preferential bonding of PH_3 molecules within the same dimer row.[77,137,139]

Wang et al. found that annealing the samples to a temperature of 950 K caused complete dissociation of the PH_x species and a simultaneous change in the overall surface morphology.[137] Whereas at low temperatures the PH_x fragments are clearly adsorbed on the flat Si(001) surface, after annealing the surface it was found that islands were observed on the surface by the substitutional displacement of P into the extended surface, ejecting Si onto the surface. Thus, the deposition of P onto Si(001) does not produce phosphorus on the surface but rather phosphorus in the extended surface plane. Increased amounts of phosphorus could be deposited either by sequential stages of 300 K exposure followed by 950 K annealing or by dosing at elevated temperature. For surfactant-type growth and heteroepitaxy applications, the structure and properties of the phosphorus-saturated surface are of prime importance. Figure 13 shows STM images of a Si(001) surface with nearly one monolayer of adsorbed phosphorus. The presence of phosphorus at these high coverages produces a very rough distribution of step edges. Many small lines can be observed, which appear to be lines of vacancy defects in the phosphorus layer. These same phenomena were later reported by Kipp et al., who attributed the lines of vacancy defects to (111) microfacets.[141] At higher resolution, Wang et al.[137] were able to resolve the individual silicon and

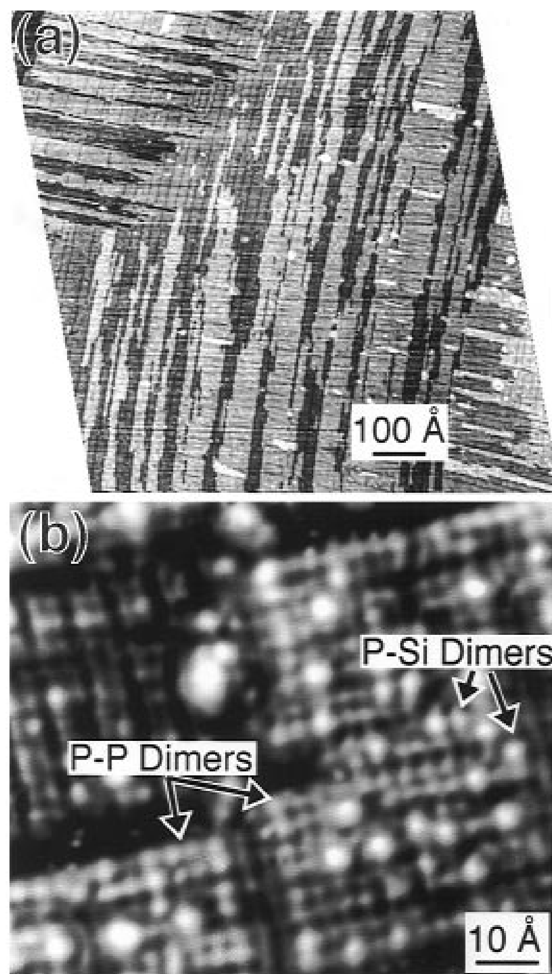

Figure 13. (a) Large-scale STM image of phosphorus-terminated Si(001) surface, showing spontaneous island formation and the presence of line defects cutting perpendicular to the dimer rows. $V_{sample} = -2.0$ V; $I_{tunnel} = 0.2$ nA; dimensions = 1150 Å × 1200 Å. (b) Atomic-resolution STM image showing detailed appearance of line defects and the characteristic appearance of P−P dimers and P−Si dimers. $V_{sample} = -0.2$ V; $I_{tunnel} = 0.2$ nA; dimensions = 80 Å × 90 Å (from ref 138).

phosphorus atoms on the surface, as shown in Figure 13b.

When P is on the Si(001) surface, there are at least three different chemical species which can form. The starting surface is composed of Si=Si dimers, in which there is a formal "double bond" between the two Si atoms. At high P coverage, we expect to find P−P dimers, in which each surface P atom forms two bonds to the underlying Si substrate and a third bond to the other P atom in the same dimer, leaving each P atom with a filled "lone pair" orbital extending into the vacuum. Finally, at intermediate coverage, we might expect to have mixed Si−P "heterodimers"; in such a heterodimer, the Si atom is formally a radical with two bonds to the underlying surface and one bond to the P atom, with one remaining electron in a dangling bond, as illustrated in Figure 14. Tunneling spectroscopy data taken on the P atoms show that the phosphorus lone pair orbitals are low in energy, so at typical STM bias voltages the P atoms appear dark and Si atoms appear bright. In Figure 13b, for example, each individual atom can be assigned to P or Si based on its apparent height.

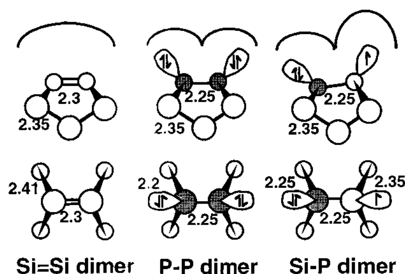

Figure 14. Structural models and bond lengths for Si=Si, P≃P, and Si−P dimers on Si(001), including top and side views (from ref 138).

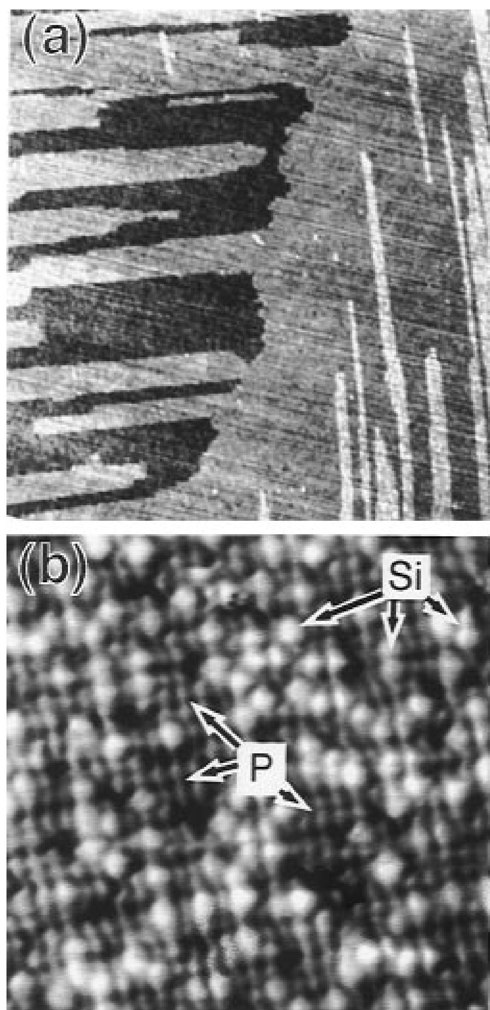

Figure 15. (a) Large-scale STM image of Si(001) surface with partial P coverage. Note the mottled appearance due to Si and P atoms and the absence of line defects. V_{sample} = −2.15 V; I_{tunnel} = 0.2 nA; dimensions = 1000 Å × 1000 Å. (b) High-resolution image of partially-P-terminated surface showing Si=Si, Si−P, and P−P dimers. Some Si=Si dimers are indicated with arrows; Si−P and P−P dimers can be found in numerous locations. V_{sample} = −2.2 V; I_{tunnel} = 0.2 nA; dimensions = 95 Å × 95 Å (from ref 138).

Because P−Si heterodimers leave one Si atom coordinatively unsaturated, it might be thought that they would undergo a spontaneous disproportionation reaction such as: 2Si−P → Si=Si + P−P to leave the surface with phase-segregated regions of Si=Si dimers and regions of P−P dimers, in analogy to the phase segregation of hydrogen, chlorine, and bromine on Si(001) into "monohydride", "monochloride", and "monobromide" structures and clean silicon. (See sections

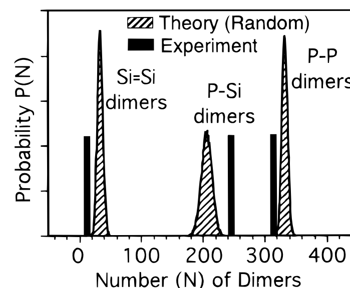

Figure 16. Statistical analysis of the surface chemical composition obtained by counting the number of Si=Si, Si−P, and P−P dimers. Black bars indicate the experimental results, while the shaded graphs show the predicted probability distribution for a completely-random alloy containing 866 P atoms and 270 Si atoms (from ref 138).

of this article on H/Si(001), halogens/Si(001), and CH_3Cl on Si(001).) In order to investigate this phase equilibrium, Wang et al. also obtained STM images at lower surface phosphorus coverages, such as the surface shown in Figure 15. Here again the Si atoms appear bright and P atoms darker, giving rise to a surface with a mottled appearance. From high-resolution images it is possible to actually count the number of Si=Si, Si−P, and P−P dimers and, from this, to estimate the energy difference between them. Figure 16 shows the experimentally-measured numbers of Si=Si, Si−P, and P−P dimers (black bars), compared with the statistical distributions that would be expected if P atoms were distributed randomly on the surface. The statistics clearly show that phosphorus does not phase segregate on the surface; instead, its distribution is nearly random, with a slight preference for forming the Si−P heterodimer compared with a random distribution. From this analysis it can be shown that the equilibrium constant for the disproportionation reaction 2Si−P → Si=Si + P−P is 0.07, implying an energy difference of ca. 5 kJ/mol or 50 meV/dimer (assuming an equilibrium temperature of ca. 500 K). Shan and Hamers[77,139] predicted an energy of 0.26 eV (0.13 eV/dimer) for the reaction 2Si−P → Si=Si + P−P using ab initio theoretical methods on a Si_9 cluster. A similar cluster was shown previously to give good results for the pairing of H on Si(001).[23,24,142,143]

The surprising stability of the P−Si heterodimers can be understood on the basis of simple strain arguments: The P−P and Si−P bond lengths are both shorter than the corresponding Si−Si bond lengths. Therefore, forming P−P dimers creates a large amount of stress at the surface. At high phosphorus coverage this high stress can only be relieved by formation of vacancy defects, as shown in Figure 13. At intermediate surface coverages, this surface stress can be relieved by forming the Si−P heterodimer.

2. Influence of Surface Phosphorus on Reaction Chemistry of Si(001)

It is widely recognized that the presence of phosphorus modifies the reaction rates and mechanisms during CVD growth of silicon[131,144−146] and silicon−germanium alloys.[147,148] Shan et al. used infrared spectroscopy in conjunction with STM measurements to show that surface phosphorus modifies the reac-

tivity of the Si(001) in two ways.[139] First, it was found that since the Si atom in the P−Si heterodimer still has a dangling bond, it can bond to a hydrogen atom, giving rise to a Si−H absorption with a frequency different from that of Si−H on the clean surface in the monohydride or hemihydride structures. By comparing the FTIR spectra as a function of temperature, Shan found that the H atoms in the form of this P−SiH "hydrided heterodimer" are bonded more strongly than H atoms on the clean surface, so that a higher annealing temperature is required to desorb them.[139] This effect was recently confirmed by Yoo et al. using temperature-programmed desorption.[149] Since adsorbed H makes the surface more passive, the increased stability of H in this chemical form makes the surface less reactive than would be anticipated based solely on the coverage of phosphorus.

A second and more interesting effect of P on the surface reactivity arises because of the way in which surface phosphorus modifies the spatial distribution of reactive surface sites. It is generally believed that most molecules of interest in CVD processing such as silane, disilane, phosphine, and diborane require two adjacent surface sites in order to react.[28,57−59,150] Because the distance between dimers is large (3.84 Å) compared with P−H, Si−H, or Si−Si bond distances, it is generally believed that the critical transition state in dissociative adsorption involves a molecular fragment simultaneously bonding to the two Si atoms within a single Si=Si dimer, which are separated by only 2.3 Å.[150] Because P distributes on the surface in the form of P−Si heterodimers, most of the surface sites have only one location (the dangling bond of a P−Si heterodimer) for attachment. Yet, this site does not provide a low-energy pathway for PH_3 dissociation due to the long distance to the nearest available Si surface site. The net result is that phosphorus present as P−Si heterodimers act as isolated reactive sites: Fragments are able to bond to the dangling bond on the Si atom but are inhibited from dissociating by the absence of a dangling bond on the other side of the same dimer. This effect can be clearly observed in infrared spectra of surfaces enriched in surface phosphorus. For example, FTIR spectra obtained after exposure of PH_3 to clean Si(001) and to Si(001) which was previously enriched with ca. 0.6 monolayer phosphorus show the formation of predominantly P−Si heterodimers. As the phosphorus concentration is enriched, it can be seen that the three peaks associated with molecular phosphorus are retained, but the PH_{2ads} and H_{ads} dissociation products are reduced.[139] This in turn implies that the presence of surface phosphorus permits adsorption of PH_3 in molecular form but prevents its dissociation. A similar effect can be observed for the interaction of disilane with P-enriched Si(001), as shown in Figure 17. On the clean surface FTIR spectra show that disilane dissociates to produce primarily SiH_2 and SiH species (in agreement with the STM observations shown above). On the P-enriched surface, however, it can be seen that the overall reactivity is lower (the spectrum has been enlarged three times) and that the higher hydrides, particularly SiH_3, are stabilized.[139] Again, dissociation is inhibited by the absence of two immediately-adjacent surface sites. Such a model for phosphorus inhibition of CVD growth is also supported by recent quantitative growth-rate studies.[147]

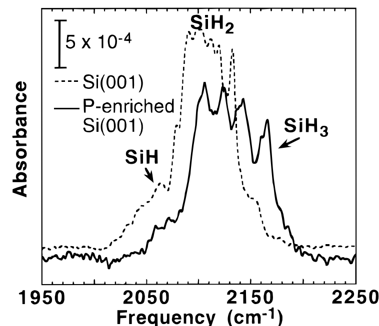

Figure 17. Infrared spectra showing the influence of surface P on the adsorption of Si_2H_6 (bottom). Surface P inhibits dissociation and leads to stabilization of SiH_3 species by changing the spatial distribution of surface sites (from refs 139 and 169).

h. Interaction of Ammonia with Si(001)

While ammonia is isoelectronic with PH_3, it has a significantly higher reactivity at 300 K. Early X-ray photoemission studies showed that NH_3 dissociates at temperatures as low as 90 K.[151−153] Ion-scattering spectroscopy showed that the H atoms reside on the surface while the N atoms are located in subsurface sites.[151] Scanning tunneling microscopy studies of NH_3-exposed Si(001) surfaces revealed atomic-level changes resulting from this dissociative adsorption.[21,45] Even at room temperature, it was shown that the NH_3-exposed surface develops a (2×1) monohydride structure, identical with that described in section IIb of this manuscript. Tunneling spectroscopy measurements showed that the NH_3 exposure leads to removal of the π bonding and π^* antibonding levels and leads to the formation of a new Si−H antibonding state at ca. 1 eV above E_F. The STM experiments did not observe any new feature that could be attributed to the subsurface nitrogen, suggesting that it does not greatly perturb the surface electronic structure. Unfortunately, the STM measurements do not provide much insight into the location or identity of the NH_x fragments produced by dissociation. Other surface science studies have generally reported the formation of NH_{2ads} and H_{ads} as the primary dissociation products at room temperature.[154−156] However, there is also some evidence for molecular NH_3 at low temperatures.[157,158]

i. Interaction of Boron Hydrides with Si(001)

While phosphorus is a prototypical n-type dopant for Si, virtually all p-type doping of Si during CVD is accomplished through the thermal decomposition of diborane, B_2H_6.[159−162] Boron has also been used as a surfactant in the growth of Ge on Si(001).[163] The many previous investigations of boron on Si have shown several interesting features. On the Si(001) surface, previous diffraction-based studies showed that surface boron retains the (2×1) diffraction pattern of the clean Si surface but with changes in the relative intensities of the diffraction spots.[135,164]

One of the most interesting properties of boron, however, is that on Si(001) boron can be used to fabricate "δ-doped" layers, in which the boron atoms are confined to nearly a single atomic plane.[160,164−168] Meyerson et al. [160] at IBM and Feldman and co-workers[164,167,168] at AT&T Bell Laboratories characterized both the structural and electronic properties of boron atoms confined in a two-dimensional δ-doped layer on Si(001). Meyerson et al.[160] and Cao et al.[166] showed that by confining boron atoms in this way, it is possible to produce electronic devices in which the boron exceeds the (thermodynamic) solubility limit by more than 2 orders of magnitude while still remaining electrically active. Under equilibrium conditions boron would be expected to precipitate as elemental boron or boron silicide. The utilization of kinetically-stable structures such as the δ-doped layers represents one possible route to overcoming the limitations imposed by "randomness" at ultra-small dimensions.

When Si(001) is exposed to diborane (B_2H_6) at room temperature, Wang et al.[169] found that dissociation occurs to first produce an adsorbed B_2H_{5ads} and adsorbed hydrogen. Further dissociation occurs on a time scale of ca. 30 min to BH_{2ads} and H_{ads}. Figure 18 shows STM images of the B_2H_6-saturated surface and an infrared spectrum taken under the same conditions. Although H_{ads} and BH_{2ads} would be expected to have different electronic structures and hence should be distinguishable in the STM, such discrimination was not found. This might perhaps arise because the Si−H and Si−B bonding states might lie far below the Fermi energy; under such circumstances, the STM images will be dominated by the dimer σ bond and might be insensitive to the nature of the adsorbates. The larger fragments were identified on the basis of the FTIR spectra as B_2H_{5ads} fragments which are stabilized by the presence of nearby hydrogen, which inhibits dissociation by a simple site-blocking mechanism.

When Si(001) is exposed to diborane (B_2H_6) at 815 K and subsequently annealed to 1000 K, STM images reveal a series of beautiful (but complicated) reconstructions. At low exposure, Figure 19a shows a new feature which can be directly associated with the presence of boron. As the surface coverage is increased, the density of these boron-induced features increases, and we also observe the formation of a new ordered reconstruction with c(4×4) symmetry. One of the most important results of this boron-induced reconstruction is that it leads to a two-dimensional phase segregation of boron on the surface, that is, at most boron coverages the surface consists of c(4×4)-reconstructed regions (with a very high local boron concentration), separated by regions of nearly-clean silicon. Thus, while phosphorus (discussed above) prefers to disperse on the surface, boron tends to agglomerate into islands, leading to a very "patchy" spatial distribution of surface boron. As shown in Figure 19b, high-resolution STM images show that the unit cell is comprised of two subunits: one bright dimer (labeled "B") and a pair of darker dimers (labeled "A"); the bright dimer (B) is sometimes absent, leaving behind what appears to be a vacancy.

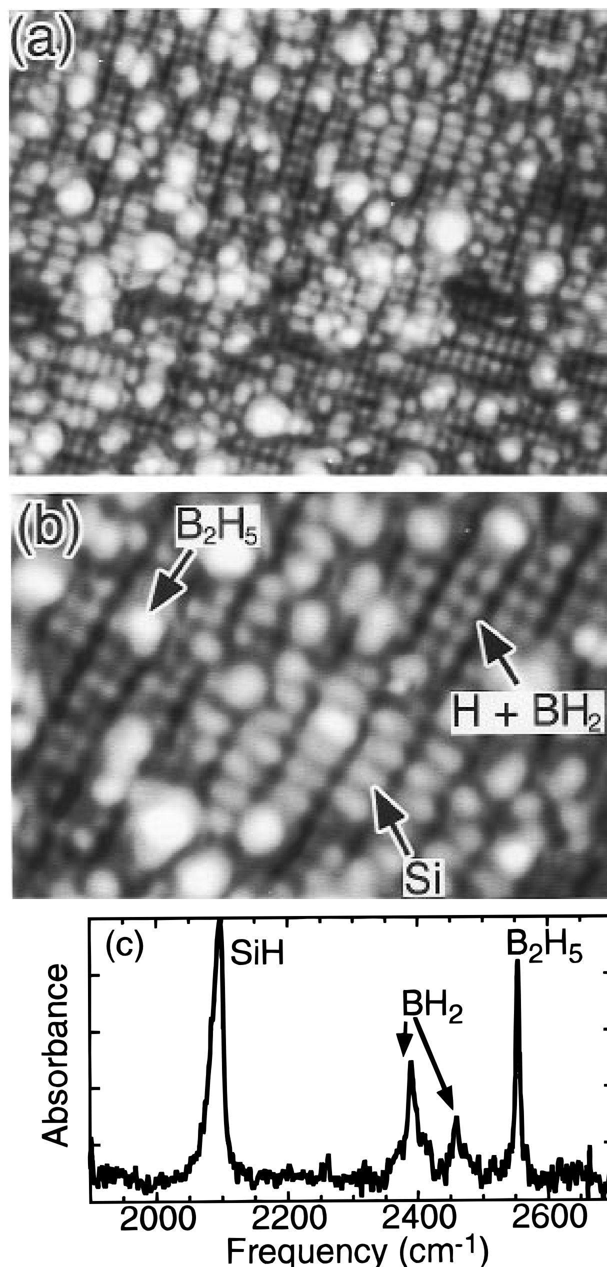

Figure 18. (a and b) STM images of Si(001) exposed to 180 langmuir of B_2H_6 at 300 K. Several patches of reacted Si regions are indicated by arrows: (a) Dimension = 170 Å × 128 Å, $V_{sample} = -3.0$ V, $I_{tunnel} = 0.3$ nA; (b) dimension = 80 Å × 55 Å, $V_{sample} = -2.0$ V, $I_{tunnel} = 0.3$ nA. (c) IR spectrum taken after exposing Si(001) to 28 langmuir of B_2H_6 at room temperature (from refs 172 and 237).

Since the STM actually probes the spatial distribution of electronic states and not the positions of the atoms themselves, inferring surface structure from STM images can be somewhat complicated. In the case of B/Si(001), Wang et al.[170] utilized several pieces of information in order to develop a structural model: First, the intensities of the characteristic Auger electron spectroscopy lines of Si and B were measured, and the fractional surface area occupied by the (4×4) reconstruction was measured with STM on the same sample; these results were then compared with analogous measurements for the $(\sqrt{3}\times\sqrt{3})R30°$ reconstruction of B on Si(111), which (as discussed below) occurs at one-third mono-

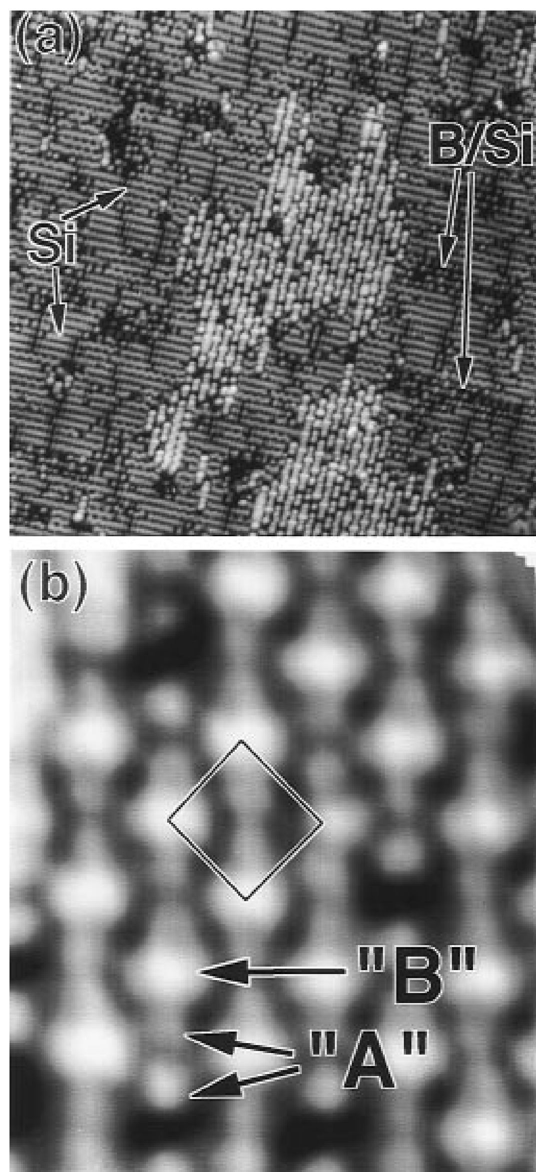

Figure 19. (a) STM image of diborane-exposed surface showing formation of reconstructed islands and patchy reconstruction of substrate terrace. $V_{sample} = -2.0$ V; $I_{tunnel} = 0.2$ nA; dimensions = 485 Å × 485 Å. (b) High-resolution image of boron-induced reconstructions on Si(001) surface. $V_{sample} = -2.0$ V; $I_{tunnel} = 0.2$ nA; dimensions = 48 Å × 60 Å (from refs 170 and 173).

layer B coverage. The result of this study showed that the local boron concentration in the c(4×4) regions was one-half monolayer. This is the same concentration at which previous studies showed that formation of the "δ-doped" B/Si(001) layers was optimized,[164,168,171] strongly suggesting that the c(4×4) reconstruction is the same structure that is responsible for the "δ-doped" layer formation. Wang et al. also obtained atomic-resolution images of the occupied- and unoccupied-state images of the reconstruction, taken over a single surface region. Through a longer analysis which has been presented elsewhere,[170] a structural model was developed for the boron-induced reconstructions which is consistent with all experimental evidence and is shown in Figure 20. In this model, boron atoms substitute into the second atomic layer and are therefore in substitutional positions. This layer is then capped with an

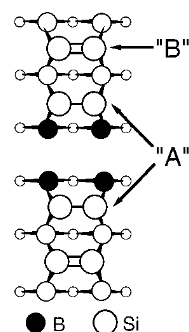

Figure 20. Structural model of boron-induced reconstruction on Si(001), showing boron atoms in second layer (black) with Si dimers on top (from refs 170 and 173).

ordered array of Si=Si dimers. There are two types of Si dimers in this model. In each unit cell there are two boron-bonded Si dimers, which are directly bonded to boron atoms, and one "normal" silicon-bonded Si dimer. The bright protrusions (labeled "B") in Figure 19 are attributed to the Si-bonded Si dimers, while the darker protrusions (labeled "A") are attributed to the boron-bonded Si dimers. Wang et al. proposed that the boron-bonded dimers likely had their weak π bond broken, transferring the electron to the boron atom; as a result, filled-state images of the boron-bonded dimers probed only the σ-bond state, which is lower in energy and less accessible to tunneling at low voltages.

One of most interesting results of the formation of a boron-induced reconstruction on Si(001) is that it also results in a spatially-varying chemical reactivity. Wang et al.[170,172,173] found that after exposure of the boron-induced reconstruction to water vapor, the B unit (silicon-bonded Si dimers) showed a splitting in filled-state images that was identical with that for H/Si(001), while the boron-bonded dimers were unaffected. On a larger scale, it was found that the reactivity of the boron-reconstructed regions was several orders of magnitude smaller than that of the clean Si(001) surface. This spatial variation in chemical reactivity has implications both for how boron affects CVD growth rates as well as for the roughness of CVD-grown B-doped Si films. To investigate the chemical reactivity, surfaces which exhibited the B-induced reconstruction were exposed to disilane (Si_2H_6) and then imaged with STM. The STM images showed that the boron-reconstructed regions were much less reactive than the "clean" regions, as shown in Figure 21. Here, individual disilane fragments can be observed on the Si(001) regions at right, while the boron-reconstructed region at left is unaffected. This difference in chemical reactivity persists at much higher exposures and at higher temperatures. Infrared spectra also showed that the reactive sticking coefficient for disilane scaled inversely with the fractional area occupied by the boron reconstructions. Wang et al. showed that the net effect of this spatially-modulated chemical reactivity was to roughen the surface during CVD growth from disilane.[174]

Although B_2H_6 is the precursor most often used for boron deposition in the microelectronics industry, its toxicity and pyrophoric nature make $B_{10}H_{14}$ (a white, crystalline powder) an attractive precursor for laboratory investigation. Wang et al. investigated the

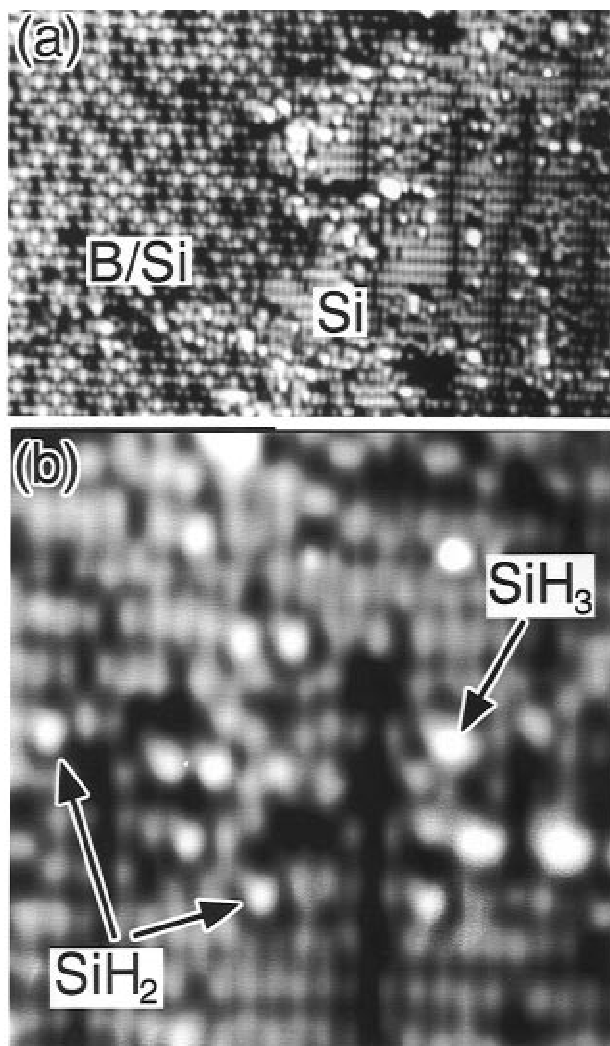

Figure 21. STM images of B/Si(001) surfaces exposed to 0.05 langmuir of Si_2H_6 at 300 K, showing the higher chemical reactivity of the clean surface (right) than the regions with the boron-induced reconstructions (left) toward disilane. Note the absence of random white protrusions in the left half of the image. Part b shows the enlarged region from the right side of part a, showing SiH_3 and SiH_2 fragments: (a) image dimensions = 380 Å × 250 Å, V_s = −2.0 V, I_t = 0.3 nA; (b) image dimensions = 90 Å × 90 Å, V_s = −2.0 V, I_t = 0.3 nA (from ref 238).

adsorption and thermal decomposition of $B_{10}H_{14}$ on Si(001). Figure 22 shows an STM image of a Si(001) surface exposed to 0.5 langmuir of $B_{10}H_{14}$. Unlike B_2H_6, which has an extremely small sticking coefficient, $B_{10}H_{14}$ sticks readily to Si(001). STM images show that the molecules have a tendency to cluster. Additionally, the STM tip is able to image some of the internal structure of the $B_{10}H_{14}$ molecule. As shown in Figure 22 the $B_{10}H_{14}$ molecule has a σ_v mirror plane; each of the molecules shows a small line running through the molecule (in random orientations). Wang et al. found that exposure of Si(001) to decaborane at elevated temperatures produced the same boron-induced reconstructions as exposure to B_2H_6, except that the long-range order was poorer with $B_{10}H_{14}$. This is believed to arise from the effectively higher dosing rate using $B_{10}H_{14}$ (because of its higher sticking coefficient), which does not allow the B-induced reconstructions to achieve long-range order as well.

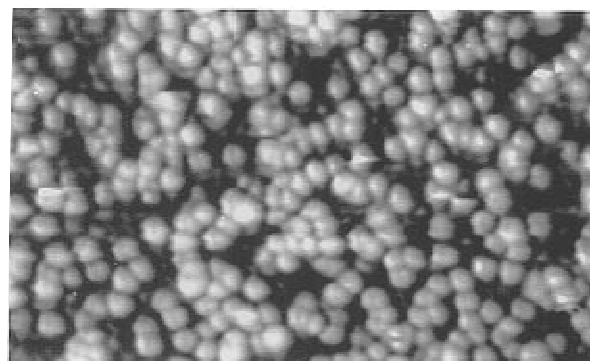

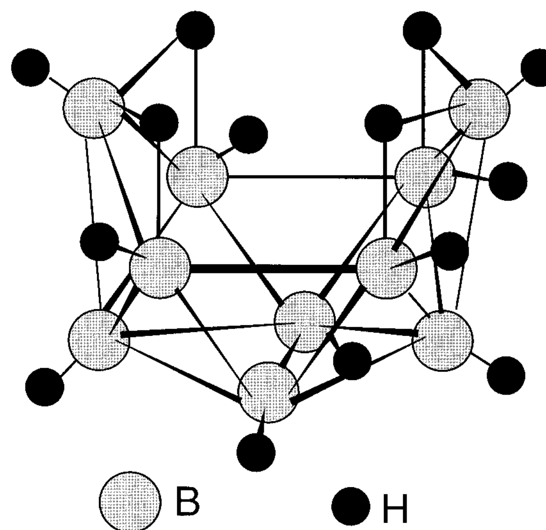

Figure 22. Image of Si(001) exposed to 0.5 langmuir of $B_{10}H_{14}$ at 300 K. Images dimensions = 150 Å × 80 Å; V_{sample} = −4.1 V; I_{tunnel} = 0.3 nA (from ref 237).

j. Interaction of Trimethylgallium with Si(001)

The reaction of trimethylgallium with arsenic compounds such as AsH_3 represents one possible route to heteroepitaxial growth of GaAs on Si(001).[175–178] Bronikowski et al.[179] examined the adsorption of trimethylgallium (TMG) with Si(001) at room temperature and elevated temperatures. At room temperature, the interaction of TMG with Si(001) is partially dissociative. As shown in Figure 23, room-temperature exposure leaves a complex-appearing surface; close inspection shows three types of surface species. Long rowlike structures are observed, which are identified as rows of gallium dimers; this observation immediately implies that the initial adsorption is at least partially dissociative. A second feature—the round, high (bright) protrusions—is dissociation fragments. When imaging the empty electronic states, STM images of these fragments show two protrusions for each fragment. On this basis, the fragments were attributed to dimethylgallium (DMG). By obtaining STM images of the same region before and after dosing the surface, Bronikowski showed that the DMG fragments were almost always bonded adjacent to defects that were present on the original surface, thus showing that defects stabilize the DMG intermediate. The third type of fragment present on the

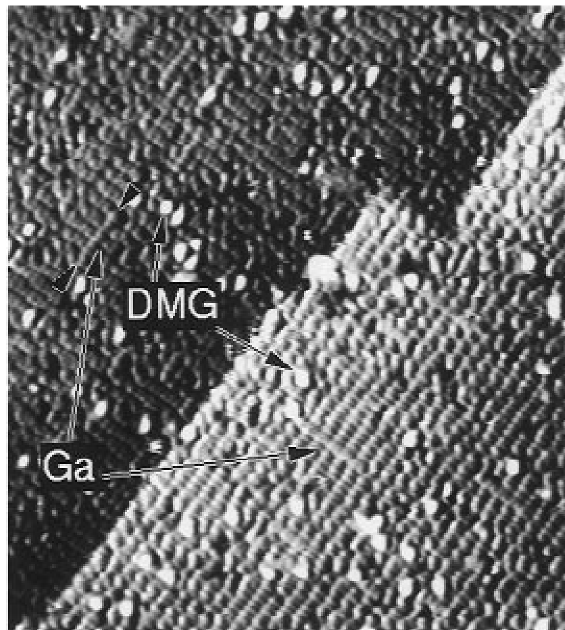

Figure 23. Large-scale STM image of a Si(001) surface dosed with ~0.2 langmuir of TMG, showing Ga strings and dimethylgallium (DMG) fragment. Dimension = 265 Å × 300 Å; $V_{sample} = -2.4$ V; $I_{tunnel} = 0.3$ nA (from ref 179).

surface is the methyl (CH_3) groups. While individual CH_3 groups are difficult to observe in Figure 23 because of the very high contrast associated with the DMG fragments, high-resolution images reveal their presence on the original surface.

As shown in Figure 24, annealing the surface to 420 K allows the $Ga(CH_3)_2$ fragments to dissociate, leaving the surface containing only CH_3 groups and Ga atoms. The Ga/Si(001) system has been investigated using a variety of experimental and theoretical methods.[180−184] All studies agree that Ga atoms on the Si(001) surface dimerize. However, the orientation of the gallium dimers with respect to the underlying Si substrate is not definitively established. Northrup[181] calculated that the most stable structure consists of Ga ad-dimers with their axis parallel to the dimers of the underlying substrate, while others[180,182−184] have suggested that the Ga dimers will have their axis rotated by 90°, analogous to a dimer of epitaxial Si. In the STM images of Ga/Si(001), each Ga dimer shows two bright elongated protrusions. It is believed that these protrusions represent the locations of the Ga−Si backbonds. If this is correct, then the STM images demonstrate that the Ga dimers are indeed oriented parallel to the underlying surface, in the geometry predicted by Northrup.[181] It is interesting to note that the Ga is able to diffuse more readily on the surface than are the methyl groups; in Figure 23, for example, the gallium dimers have already aligned into rows at room temperature, while the methyl groups are not ordered.

The methyl groups produced by dissociation of TMG appear in STM images as dimers which uniformly appear higher than the underlying substrate, with one of the ends being higher than the other; these are shown in Figure 24b. This contrast is qualitatively similar to the contrast generated by individual SiH_{3ads} groups discussed above, but the contrast between CH_{3ads} and the clean surface is smaller. For both CH_3 and SiH_3, it must be remembered that because the STM images the surface electronic structure, it cannot be definitely established whether the protrusion corresponds to the dangling bond left on the other Si atom of the dimer pair or if it corresponds to the location of the SiH_3 or CH_3 group. It is clear from a comparison of CH_3 and SiH_3, however, that the appearance of even isoelectronic fragments in the STM is different. This effect might be related to the fact that the dangling bond of the unbonded Si atom in the dimer can act as a reservoir of charge; small differences in the amount of charge transfer between the adsorbate (SiH_3 or CH_3) and the underlying surface might then give rise to correspondingly large changes in the electronic-state density near the Fermi energy.

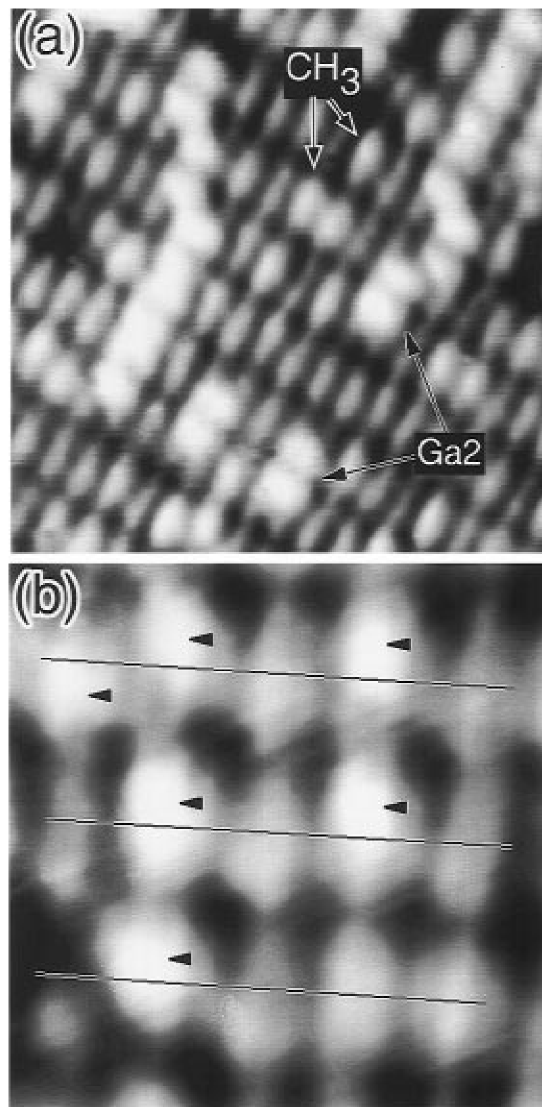

Figure 24. STM images of a Si(001) surface dosed with 0.2 langmuir of TMG and then heated to 425 K for 2 min, showing "CH_3" and "Ga_2" features: (a) image dimensions = 123 Å × 123 Å, $V_s = -2.4$ V, $I_t = 0.3$ nA; (b) high-resolution STM image, showing individual CH_3 fragment. Image dimensions = 25 Å × 25 Å; $V_s = -2.4$ V; $I_t = 0.3$ nA (from ref 179).

k. Interaction of Methyl Chloride with Si(001)

Bronikowski et al. investigated the interaction of methyl chloride with Si(001).[91] One motivation for

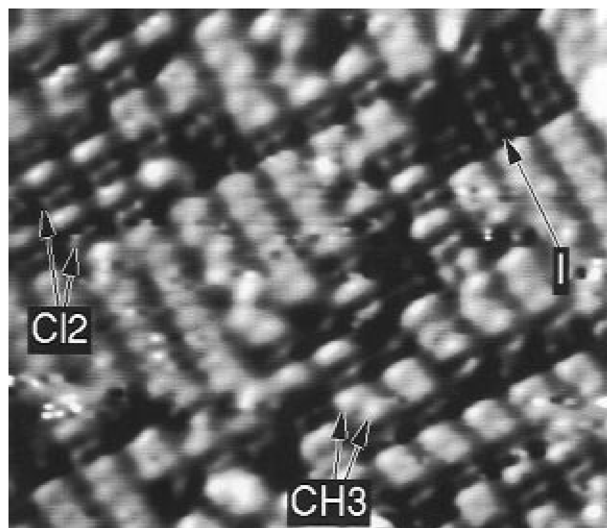

Figure 25. High-resolution STM image of a Si(001) surface dosed with 0.3 langmuir of methyl chloride and then heated to 425 K for 2 min, showing "CH_3", "Cl_2", and "I" features. Area = 90 Å × 75 Å; $V_s = -2.2$ V; $I_t = 0.3$ nA (from ref 91).

investigating CH_3 species is that, since it is isoelectronic with SiH_3, a comparison of the STM images resulting from these two fragments provides some insight into the application of STM to identify unknown molecular fragments. Additionally, the chemistry of CH_3 and CH_2 groups is fundamentally important to the epitaxial growth of SiC on Si(001) and to the nucleation of diamond in a number of systems.

The work of Bronikowski et al.[91] focused on samples prepared by exposing Si(001) to CH_3Cl at room temperature followed by a brief anneal at 420 K. Since previous studies using methyl iodide have shown that methyl groups are stable up to 600 K,[185,186] the only species present on the surface after this exposure−anneal cycle should be Cl and methyl groups. The Cl atoms produced by dissociation pair onto the Si(001) dimers, forming a "monochloride" structure identical in all respects with that observed by Boland.[92] After the 420 K anneal, the Cl atoms formed small islands of the monochloride structure with diameters on the order of 20 Å. These regions of monochloride can be observed readily in Figure 25. As noted above, identification of methyl groups from molecules like methyl chloride and trimethylgallium is difficult because of low contrast but is possible. The methyl groups bond to a dimer dangling bond.

I. Interaction of Ethylene and Acetylene with Si(001)

Understanding the behavior of hydrocarbons and other organic molecules on silicon surfaces is of interest in a number of areas, including the growth of β (cubic) SiC and the general use of organic-derived molecular precursors for semiconductor processing.[187−189] The π-molecular system of unsaturated hydrocarbons such as ethylene, acetylene, and propylene makes them particularly reactive with Si(001).[187] Quantitative coverage measurements by Cheng et al.[190,191] showed that both ethylene and acetylene adsorb with a saturation coverage of 2.5 × 10^{14} molecules/cm^2, compared with the Si(001) atom density of 6.8 × 10^{14}/cm^2, or 3.4 × 10^{14} dimers/cm^2. Cheng et al. proposed that defect sites would be less reactive, so that the saturation coverage on the nondefected surface areas was likely 1 hydrocarbon molecule/dimer site. They also proposed that both ethylene and acetylene adsorbed on Si(001) in a di-σ configuration in which the π system of the unsaturated carbon is aligned with the π system of the surface dimers, forming the four-atom ring structure depicted in Figure 26. Mayne et al.[192,193] investigated the adsorption of ethylene on Si(001) with STM and confirmed that the ethylene molecule does bond directly on top of the Si(001) dimers in the di-σ configuration. However, Mayne found that ethylene molecules adsorbed only on every second Si dimer, giving rise to a saturation coverage only one-half that found earlier by Cheng.[190] Mayne et al. also observed ordering between adjacent rows then naturally leads to (2×2) and c(4×2) reconstructions. The apparent discrepancy in coverage can be resolved if it is assumed that defect sites are actually more reactive (not less, as proposed by Cheng) than the clean surface; on this basis one could argue that the coverage on defect-free surface areas is 1.7 × 10^{14} molecules/cm^2, in agreement with the observations of Mayne. The reversibility of the adsorption of ethylene is demonstrated by the fact that after annealing the sample Mayne et al. found desorption of molecular ethylene and the restoration of the clean Si(001) surface. On the basis of isotopic mixing temperature-programmed desorption experiments using ^{12}C and ^{13}C, it was found that there was <1% mixing between the isotopes. The absence of isotopic mixing implies that the ethylene molecules which desorb do not arise from recombinative desorption but instead are produced by a reversible adsorption−desorption of intact ethylene molecules. While it is clear the ethylene adsorbs molecularly in the di-σ-bond configuration, one important question not yet resolved is whether the σ bond of the silicon dimer is intact (as depicted in Figure 26) or broken. High-resolution electron energy loss spectroscopy studies[189] suggest that the silicon σ bond is intact; however, Taylor and co-workers[191] have argued that this would be expected to produce a high degree of strain in the silicon lattice and suggest that the σ bond is broken.

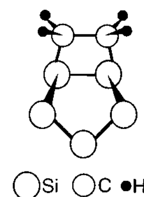

Figure 26. Structural model of the adsorption site of di-σ-bonded C_2H_4 on Si(001). The silicon dimer σ bond is depicted as intact, with the π bond broken.

While acetylene has the same saturation coverage as ethylene and both molecules can bond to Si(001) in a di-σ configuration, Mayne et al. found that the adsorption of acetylene (ethyne) on Si(001) produces a somewhat disordered surface.[193] More work is needed on this system to unambiguously establish the mode of adsorption and bonding on Si(001).

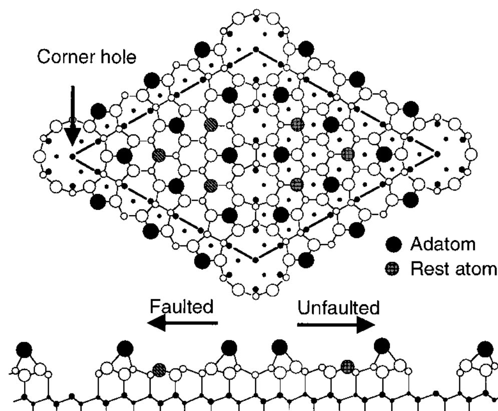

Figure 27. Structural model for Si(111)-(7×7) "dimer–adatom–stacking fault" model (from ref 194).

III. Atomic-Level Studies of the Chemistry of Si(111)

Despite the fact that silicon-based microelectronic devices are formed exclusively on the (001) crystallographic plane, the Si(111) surface has enjoyed a great deal of interest. The intense study of this surface has been motivated by several factors. (1) It is the thermodynamically most stable crystal face. (2) It has an intriguing (7×7) reconstruction whose atomic structure defied structural analysis for many years. (3) For STM investigations, the large unit cell and unusually large corrugation make it easy to image, while the comparative insensitivity to surface contamination makes it easier to prepare. (4) The (now) known structure of this surface provides a rich array of chemically-inequivalent atoms, resulting in a rich variety of chemically-interesting and spatially-inhomogeneous chemical reactions.

a. Structure and Bonding of the Si(111)-(7×7) Surface

The reconstruction of the Si(111) surface has been widely studied with a large number of experimental techniques. The now accepted model for Si(111)-(7×7) is the dimer–adatom–stacking fault (DAS) model proposed by Takayanagi et al.[194] as shown in Figure 27. In the bulk diamond structure (also adopted by bulk silicon and germanium), the (111) surfaces are arranged in "double layers". Each double layer contains two sets of atoms separated vertically by 0.78 Å, while the (center-to-center) separation between double layers is 3.13 Å. In the DAS reconstruction, the stacking sequence near the surface is modified such that the surface contains triangular regions of faulted and unfaulted regions; dimers serve as "zippers" to join the faulted and unfaulted regions. At the position where the apexes of the triangular regions join, there is a deep "corner hole". Finally, the surface layer is capped with a layer of 12 adatoms.

As shown in Figure 27, the structure of the Si(111)-(7×7) surface presents at least five chemically-distinguishable types of surface atoms. The adatoms in the faulted and unfaulted halves are inherently different, and within each half the three adatoms nearest the deep "corner hole" are different from the remaining three. There are also seven "rest atoms",

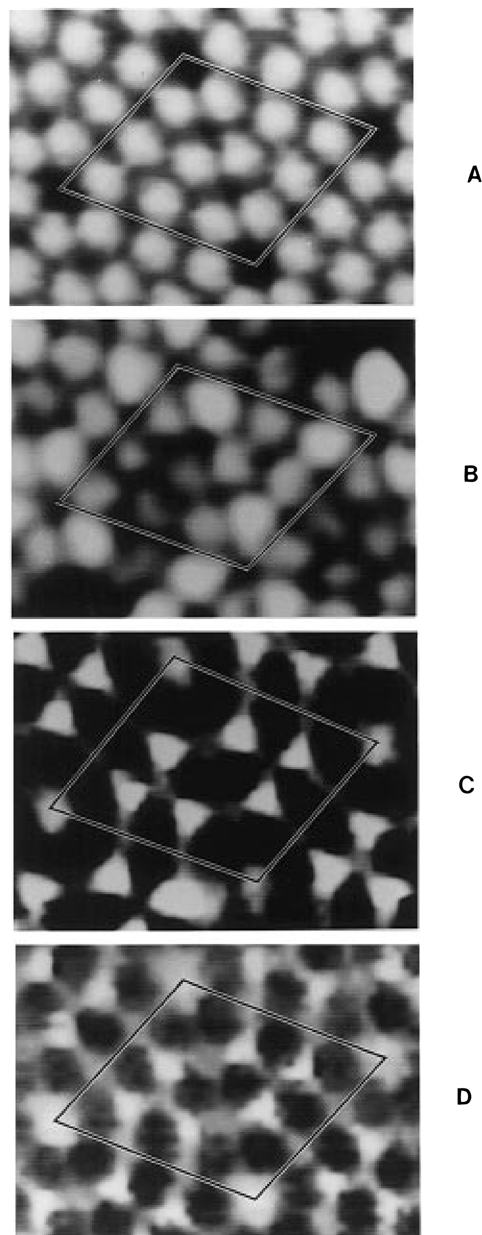

Figure 28. STM and current imaging tunneling spectroscopy measurements of Si(111)-(7×7) surface, showing surface topography and spatial location of different surface states: (a) topographic image, acquired with $V_s = 2.0$ V, (b) dI/dV map showing the adatom state at 0.35 eV below E_F, (c) dI/dV map showing the rest atom state at 0.8 eV below E_F, and (d) dI/dV map showing the backbond state at 1.7 eV below E_F.

one of which is at the bottom of the corner hole. Figure 28 shows that these differences are readily distinguishable in STM images because the chemically-inequivalent Si atoms also possess different electronic state densities. By measuring the tunneling current as a function of voltage while imaging the surface, it is possible to perform atomic-resolution surface spectroscopy and to directly image the spatial distribution of electronic states of the Si(111)-(7×7) surface.[18,195] While Figure 28a shows a conventional topographic image of the Si(111)-(7×7) surface (with one unit cell outlined), Figure 28b shows an STM image probing the electronic state density at 0.35 eV below the Fermi level; in this panel the six adatoms nearest each corner hole appear brighter than those

not adjacent to a corner hole, and the six adatoms in one half (the faulted half, constituting the right half of the unit cell in Figure 28b) are brighter than those in the other half (the unfaulted half). Thus, there are four types of chemically-inequivalent adatoms (corner faulted, corner unfaulted, center faulted, and center unfaulted), with the corner adatoms in the faulted half having the highest density of electronic states near the Fermi energy. At bias voltages near −0.8 eV, the STM probes the filled electron pair on the rest atoms, which can be viewed in Figure 28c. Finally, at bias voltages near −2.0 V (Figure 28d), the STM can reveal the locations of the backbonds between the Si adatoms and the underlying Si layer.

As on Si(001), the chemical reactivity of Si(111)-(7×7) is connected with its geometry and electronic structure. It has been noted that the Si(111)-(7×7) reconstruction has a smaller number of "dangling bonds" arising from Si atoms with a coordination number of <4 than any other proposed model for the reconstruction of Si(111). Thus, it appears that the strongest driving force for the formation of this very complicated reconstruction is the minimization of dangling bonds. As on Si(001), the minimization of dangling bonds comes at the expense of bond strain associated with deviations from perfect tetrahedral symmetry and ideal Si−Si bond lengths. The result of this bond strain is an inherent spatially-modulated chemical reactivity.

b. Interaction of H with Si(111)

Like Si(001), the Si(111)-(7×7) is unreactive toward H_2 but reactive toward atomic hydrogen. At first, the logical structure of H-saturated Si(111)-(7×7) would be for each of the 12 adatoms, the 6 rest atoms, and the dangling bond at the corner hole to bond to one H atom. This structure would give all Si atoms a coordination number of 4.

STM images of the H-exposed Si(111)-(7×7) surface have provided some disparate results.[51,196−198] Both Sakurai and co-workers[196] and Mortensen et al.[197] investigated the interaction of atomic H with Si(111)-(7 × 7) at low coverage (ca. one-fourth monolayer). In these studies, identification of reacted sites is based on the fact that while the adatoms of the clean surface have a high density of states near the Fermi energy (resulting from the formal "dangling bond"), the interaction with H reduces the state density near E_F through the formation of low-lying Si−H bonding states and high-lying SiH* antibonding states, in a manner similar to the aforementioned Si(001)-(2×1) monohydride structure. In STM images, then, the Si(111) sites that have reacted with atomic H appear dark. At coverages on the order of one-fourth monolayer, both groups found that the H atoms interacted with the "dangling bond" of the 12 adatoms within the unit cell. Both groups performed statistical analyses to show that there was no difference in reactivity between the four inequivalent types of adatom structures. This might be rationalized by assuming that the impinging H atoms react wherever they land and do not diffuse sufficiently far to explore the complete potential energy surface provided by the large Si(111)-(7×7) unit cell. At these low coverages, then, the surface consists of an intact Si(111)-(7×7) unit cell, with each Si adatom bonded to one H atom.

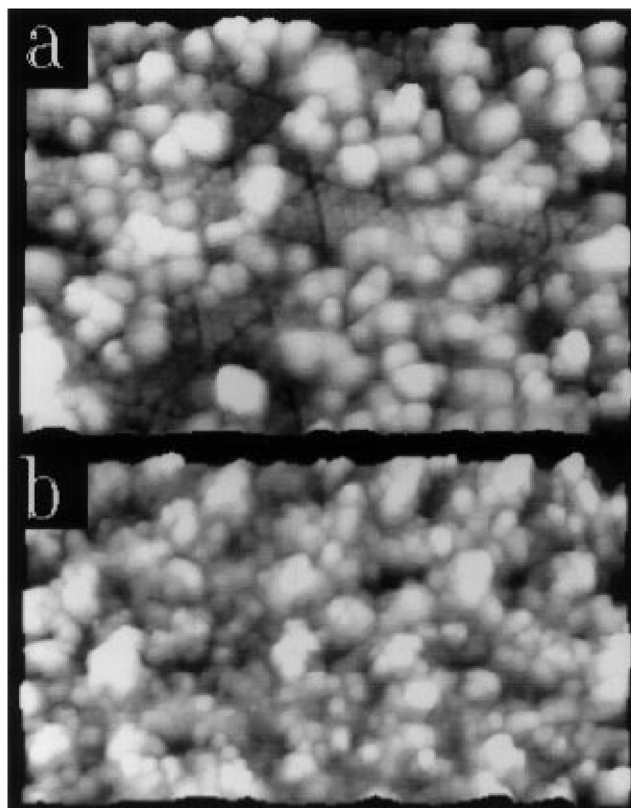

Figure 29. (a) STM image of Si(111) surface after a 300 K saturation H dose, 230 Å × 130 Å. (b) 200 Å × 122 Å image following a 5 s annealing at 690 K. Sample bias was 2 V (from ref 69).

At higher exposures, Boland[51,198] and Mortensen et al.[197] found yet another structural change involving a modification of the adlayer. In this exposure regime, H begins to insert into the backbonds between the Si adatoms and the rest atom layer. The fissioning of this bond leaves adsorbed SiH_2 and SiH_3 species on the surface of a H-terminated rest atom layer. Boland found that the SiH_x species were mobile on the surface and that they would often agglomerate into island structures, as shown in Figure 29a. In cases where individual fragments could be observed, it was found that the registry of the fragments with respect to the underlying lattice was consistent only with their identification as SiH_3 groups (i.e., a trihydride phase).

Boland also investigated the desorption of hydrogen from H-terminated Si(111) surfaces.[46,47,51,198,199] During desorption of hydrogen from Si(111), there are two desorption features, one with a maximum at 680 K due to desorption of H_2 from SiH_2 and SiH_3 species and a second at 810 K due to desorption of H_2 from monohydride (SiH) species.[60,61,200−202] Figure 29b shows an STM image of Si(111) after a 5 s anneal at 690 K, just above the β_2-peak temperature. Under the conditions used to obtain Figure 29b, the agglomerated adspecies are able to undergo successive hydrogenation reactions to produce SiH_3. Since there are only 12 adatoms in the Si(111)-(7×7) unit cell, while a bulklike layer contains 49 atoms, the Si(111) surface after exposure to large amounts of hydrogen consists of monohydride units in the surface plane, decorated with adsorbed trihydride units occupying $^{12}/_{49}$ of the surface area. While mass spectroscopy

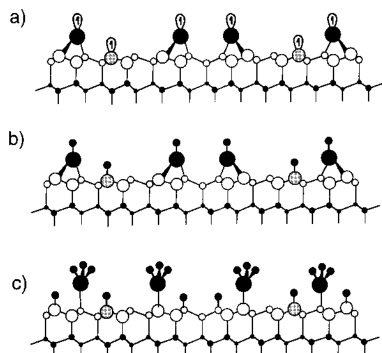

Figure 30. Structural model showing the adsorption of H on Si(111).

studies[61,203] have detected SiH_4 as a product during exposure of Si(111)-(7×7) to atomic hydrogen, the STM studies did not observe etching via the removal of SiH_3 groups. This suggests that the activation barrier to this process is quite high and that the partial adlayer of SiH_3 groups is at least kinetically stable. Annealing removes most of the SiH_2 and SiH_3 fragments but leaves the surface somewhat disordered.

It should be noted that the bond strength of Si–H is higher than that of Si–Si,[29] so that hydrogen etching would be expected to be thermodynamically favored. However, for a normal Si layer the activation barrier for this process is apparently very high, as none of the studies reported any significant etching of the Si surface. However, it is clear that the backbonds between the adatoms and the underlying rest atom layer are readily broken by H. Both studies attributed this higher rate of H atom insertion into adatom backbonds as a result of the strain associated with the adatom bonding. Figure 30 summarizes the sequential steps in the interaction of H with Si(111) at room temperature.

Boland found that after annealing H-saturated surfaces to 550 K (below the temperature for H desorption), a third structural transformation occurred, this time involving the alternating faulted–unfaulted arrangement characteristic of the (7×7) reconstruction. As shown in Figure 31, mild annealing of the surface increases the fraction of surface having the unfaulted stacking sequence, at the expense of the faulted regions. Thus, the surface reverts to a more bulklike stacking sequence. In the STM images, the differing sizes of faulted and unfaulted regions cause the dark lines demarking the edges of the unit cells to vary in position, instead of being perfectly straight as on clean Si(111)-(7×7). The reversion of the surface to a bulklike stacking sequence is quite reasonable when one considers that the driving force for the (7×7) reconstruction of the clean surface appears to be the minimization of the number of dangling bonds. The chemical energy associated with a coordination number of <4 drives the surface to reconstruct; however, the reduction in the number of dangling bonds is partially offset by the fact that the Si atoms cannot adopt their "ideal" bond lengths or bond angles, building in a strain energy. With hydrogen present to saturate the dangling bonds, all surface atoms can adopt 4-fold coordination. Under these conditions the driving

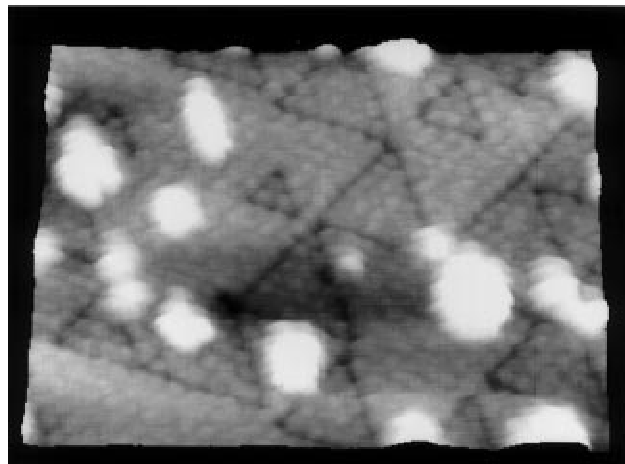

Figure 31. STM topograph of the Si(111)-(7×7) surface following a brief 550 K anneal of the saturated surface. The strained rest layer dimer rows are progressively eliminated, and a more bulklike structure is formed. Note that the reaction has not proceeded beyond the rest layer. The area shown is 92 Å × 100 Å. The dark appearance of the subunit at the center of the image is an artifact of the background subtraction (from ref 199).

force for formation of the (7×7) reconstruction is eliminated; in fact, the strain associated with this reconstruction now begins to dominate, acting as a driving force for the structure to revert back to the bulklike stacking sequence, although at room temperature this process is apparently very slow because of the low mobility of the atoms. Annealing at 550 K provides higher mobility for Si atoms, thereby allowing the surface to adopt a more bulklike stacking sequence.

c. Interaction of Silane with Si(111)

Silane is the primary precursor used in microelectronics for deposition of silicon.[28,56,57,59,79,150] Memmert and co-workers[204] found that the interaction of silane with Si(111)-(7×7) exhibits significant site selectivity. Figure 32 shows STM images of Si(111)-(7×7) exposed to silane at 300 K. It can be seen here that the adatoms immediately adjacent to the corner holes are affected first, appearing darker than the unreacted adatoms. Each corner hole of Si(111)-(7×7) is surrounded by six equivalent adatoms. Surprisingly, it was found that after only one of these six equivalent adatoms reacted, the remaining five were almost completely unreactive. Thus, after exposures of ca. 180 langmuir, it was found that virtually every corner hole was surrounded by exactly one reacted adatom, while the other five "corner" adatoms and the six "interior" adatoms remained unreacted. Although previous studies of oxygen and some other adsorbates on Si(111)-(7×7) have also shown a significant preference for reaction at the corner adatom sites, no other study has shown such a striking halt after reacting with only one of these (nearly) equivalent sites.

Although the adsorption of SiH_4 is expected to produce both H_{ads} and SiH_{3ads}, Memmert et al. observed only one type of reacted site. When the SiH_4-dosed Si(111)-(7×7) sample was annealed, however, Si islands appeared on the surface, with the number of atoms in these islands roughly corre-

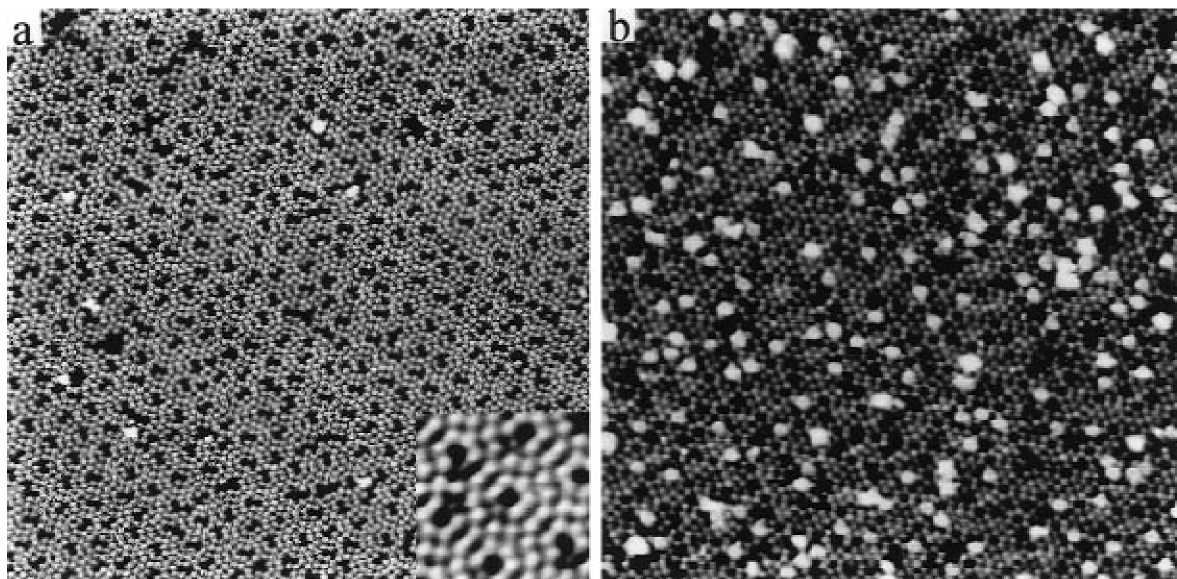

Figure 32. STM images of a Si(111)-(7×7) surface after room temperature exposure to 180 langmuir of SiH_4: (a) 500 Å × 500 Å image, recorded directly after exposure, and (b) 400 Å × 400 Å image, recorded after annealing to 800 K for 2 min (from ref 204).

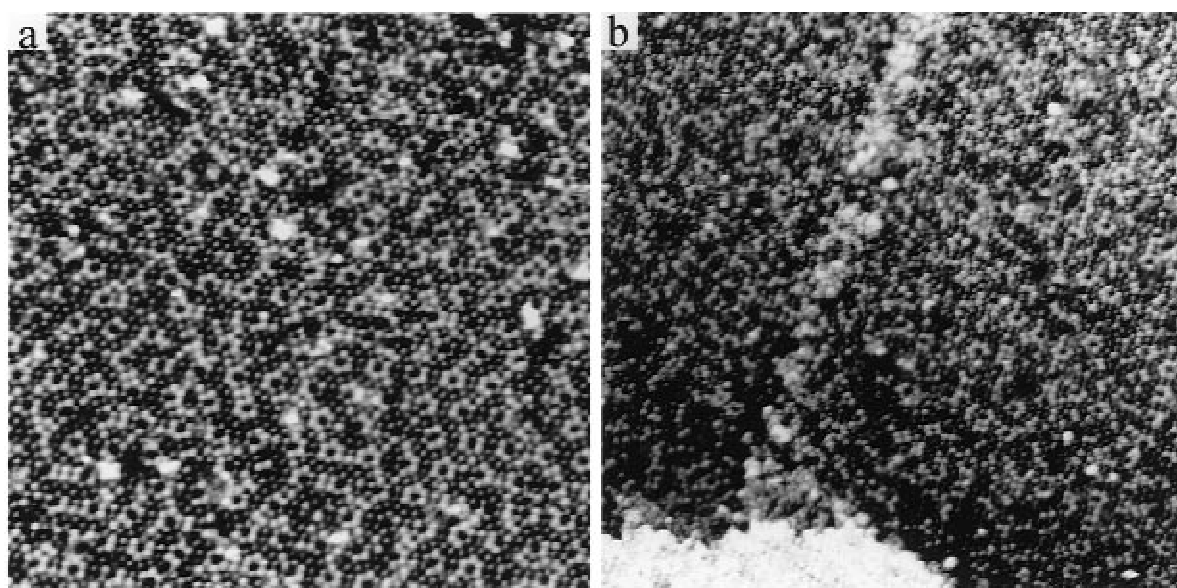

Figure 33. STM images of a Si(111)-(7×7) surface after prolonged room-temperature exposure to SiH_4: (a) at 12 000 langmuir (400 Å × 400 Å) and (b) at 18 000 langmuir (500 Å × 500 Å) (from ref 204).

sponding to the number of reacted adatoms present on the initial surface; this indicates that for each reacted "dark" adatom, there must be one SiH_3 group present as well. Where is this SiH_3 group? Memmert et al. proposed that the SiH_3 group is bonded to the dangling bond located at the bottom of the corner hole of the (7×7) reconstruction. Thus, the dissociative adsorption of SiH_4 produces one SiH_3 group at the bottom of the corner hole and one H atom bonded to one of the immediately-adjacent adatoms. Thus, the corner hole dangling bond is a "special site" for the initial reaction of Si(111)-(7×7) with SiH_4. Once this special site is filled, the reactivity of the corner hole (and the adjacent adatoms) decreases, so that only one of the six adatoms around a corner hole will react initially.

Once this phase of the reaction was complete, Memmert et al. reported that SiH_4 molecules continued to adsorb with a 50 times smaller reaction probability but that now the reaction favored H atoms adsorbed on one of the six "center" adatoms in each unit cell, as shown in Figure 33. Although it was not possible to determine if SiH_3 groups were adsorbed on the rest atom sites (analogous to the corner hole), it was noted that under these conditions small protrusions consisting of small groups of SiH_x species were also present on the surface, which could account for the deposited silicon.

One particularly-enlightening observation that was made regarding the initial stage of reaction of SiH_4 with Si(111)-(7×7) is that, although there is clearly a large difference in reactivity between corner adatoms and interior adatoms, there was very little difference between adatoms in the faulted and unfaulted halves of the unit cell. This is surprising in light of other studies such as O_2 on Si(111)-(7×7),[205–208] where the reactivity was found to be closely connected with the electronic density of states nearest

the Fermi energy. Memmert et al. attributed the differences in reactivity between corner and center adatoms to a purely-statistical factor associated with the fact that adsorption of SiH_4 on Si(111) requires two adjacent reactive sites. While in the initial stage these are the corner hole dangling bond and one corner adatom, in the second stage the reaction requires one "rest atom" dangling bond and one adatom. Since each rest atom is surrounded by two center adatoms and only one corner adatom, one would expect a 2:1 preferential reactivity for center adatoms, in agreement with the observations of Memmert.

d. Interaction of GeH_4 and Ge_2H_6 with Si-(111)-(7×7)

A strong site-selective chemical reactivity has also been observed for GeH_4 and Ge_2H_6 on Si(111).[209,210] Although results were not reported for small exposures, at moderate exposures (>3000 langmuir), preferential reactivity of the interior (center) adatom sites was observed at a substrate temperature of 640 K. It was found, however, that the reacted regions consisted not of H-terminated atoms but instead a H-terminated rest atom layer; this implies that the original Si adatoms were removed from the vicinity either by desorption or by diffusion to other regions. Indeed, some island structures were found on the surface and attributed to these agglomerated SiH_x species from the adatom removal. Since H is known to be mobile at 640 K, it was not possible to conclude whether the H atoms initially reacted at the center adatom sites or whether the reaction occurred elsewhere and the H atoms diffused to these sites. It was proposed that the SiH_x species in these islands might lead to desorption of hydrogen as well as to possible etching in the presence of excess hydrogen.

When Si was exposed to GeH_4 at higher temperatures, some qualitatively-different behavior was observed. After annealing to 700 K, no dark sites were observed, and most of the surface adopted a (7×7) or (5×5) reconstruction; however, some regions of $(\sqrt{3}\times\sqrt{3})R30°$ symmetry were also observed. Similarly, large regions of $\sqrt{3}$ were observed after dosing with Ge_2H_6 at low temperature following by annealing to 700 K. Careful studies showed that the $\sqrt{3}$ structure formed at a temperature of 643–658 K, which is the same temperature at which hydrogen desorbs from the Ge/Si(111) surface. Wintterlin et al.[209,210] proposed that there was perhaps a SiH or GeH intermediate present during the thermal composition; such an intermediate would need three more bonds to achieve optimal coordination and might therefore behave much like a group III element, which typically forms simple adatom structures with $(\sqrt{3}\times\sqrt{3})R30°$ local symmetry. This metastable $\sqrt{3}$ structure was stable up to about 875 K, above which the (7×7) reconstruction was restored.

e. Interaction of Halogens with Si(111)

In a manner similar to hydrogen termination of the adatom backbonds, Boland and Villarrubia[211,212] showed that the interaction of chlorine with Si(111)-(7×7) first produces Cl-terminated adatoms. While in general it is difficult to directly identify the chemical species present during chemical reactions with the STM, Boland's work nicely illustrates how one can sometimes obtain this information from atomic-resolution images, using the fact that Si species typically adopt an overall coordination number of 4. In the case of the Cl-terminated adatoms, the location of the SiCl group is in an adatom position, with three bonds to the underlying surface. This location can be unambiguously established from the local symmetry of the STM images. As shown in Figure 34a, lines drawn along the rows of adatoms show that the SiCl group is located in an adatom position. Upon further exposure to chlorine, the chlorine inserts into one of the backbonds between the adatom and the rest atom layer. As shown in Figure 34b, the grid lines now show that the adatom has adopted a bridge-bonded position in which it bonds to two rest atoms (and two Cl atoms). Finally,

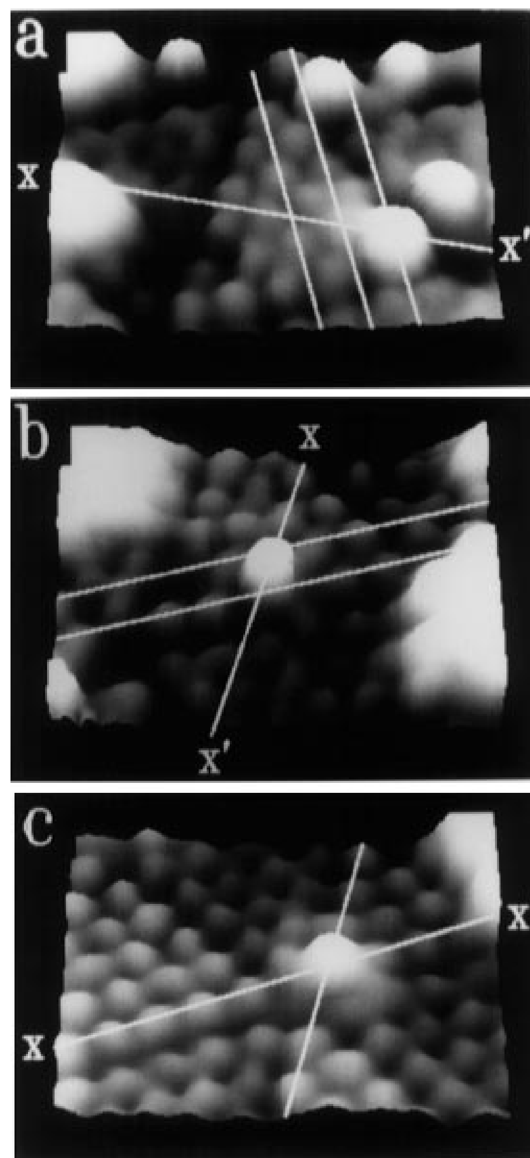

Figure 34. Three-dimensional rendering of STM topographs recorded at 2 V showing (a) SiCl, (b) $SiCl_2$, and (c) $SiCl_3$ species. The area shown is 40 Å × 29 Å. Lines have been ruled along rows of atoms to aid in the location of the adatoms on the surface. Note that rendering necessarily redistributes the adatom intensities in the tilt direction (from ref 211).

Figure 34c shows that further exposure to Cl_2 causes yet another insertion reaction, breaking one of the bonds between the chlorinated adatom and the rest atom; this in turn produces a $SiCl_3$ group which is bonded directly above a rest atom layer. At saturation coverage, X-ray photoelectron spectroscopy data show that SiCl, $SiCl_2$, and $SiCl_3$ species are all present simultaneously.[213] After annealing to 675 K, the surface shows a significant restructuring that is similar to what is observed for hydrogen: The rest atom layer is exposed, with all atoms terminated by Cl, and the adatoms consist of higher $SiCl_x$ species agglomerated together into small islands.

Feltz et al.[214] studied the interaction of Si(111) with Cl_2 at even higher temperatures, through the well-known (7×7)−(1×1) phase transition.[215,216] Direct images of the (7×7)−(1×1) phase transition at 1100 K were first obtained by Telieps and Bauer, using the newly-invented low-energy electron microscope.[216] On the clean surface, the phase transition nucleates at the upper edge of steps and then propagates across the terraces. In the presence of chlorine (by continuous exposure to Cl_2 while imaging at elevated temperatures), Feltz and co-workers observed that the (7×7) reconstruction appeared to "dissolve", beginning at the lower edges of steps and at boundaries between different domains of the Si(111)-(7×7) reconstruction on the terraces. Although images obtained at elevated temperature were not able to directly image a (1×1) structure, experiments in which the sample was quenched to room temperature succeeded in showing that the "dissolved" regions in fact consisted of (1×1) domains. Once the surface was covered with the (1×1) structure, the Cl_2 exposure could be removed, and the recovery of the (7×7) reconstruction again imaged at elevated temperature, in real time. The removal of Cl_2 and subsequent formation of the (7×7) reconstruction are now initiated at the upper step edges. Thus, the (7×7)−(1×1)−(7×7) sequence appears to follow the principle of microscopic reversibility, since the nucleation events for the (1×1)−(7×7) and (7×7)−(1×1) transitions are the exact reverse of each other.

f. Interaction of Oxygen with Si(111)

STM studies of the oxidation of Si(111) reveal some of the general difficulties in interpretation of STM images.[205−208] Investigations by Pelz and Koch[206,207] and Lyo et al.[208] both show that the exposure of Si(111)-(7×7) to O_2 produces two new kinds of surface features. One kind of O_2-induced feature is an adatom which appears brighter (i.e., higher) than the other adatoms of the same type (remembering that there are four inherently-inequivalent types of adatoms); this feature is called a "bright" site. A second O_2-induced feature is an adatom which appears darker than the normal ones and is called a "dark" site. While all three studies[205−208] reported observing the dark sites, only two of them reported also seeing the bright sites at the initial stages of oxidation. Figure 35 shows STM images of Si(111) immediately after exposure to O_2 (Figure 35a) and after sequential annealing cycles (b and c), showing how the bright sites are converted to dark sites by thermal annealing.

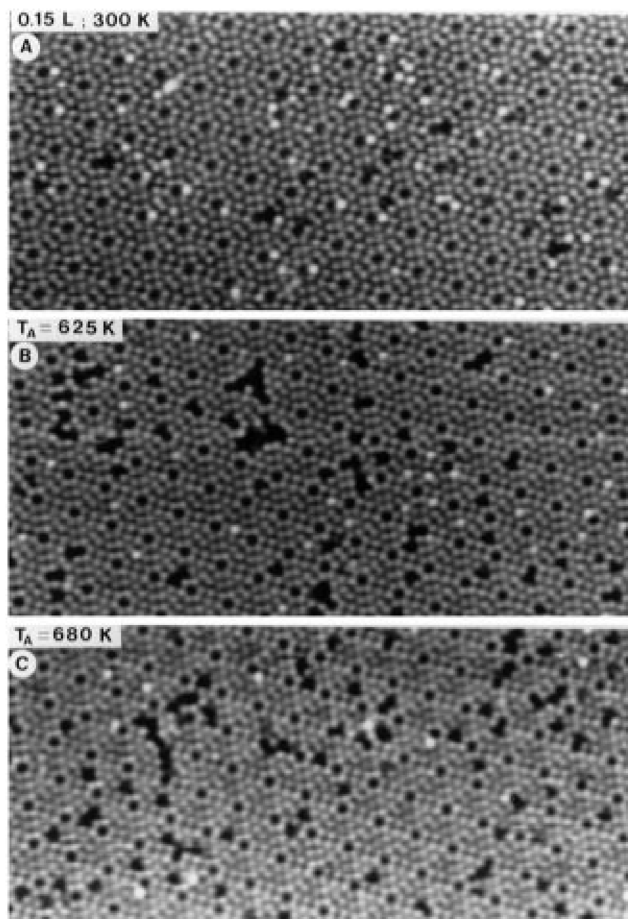

Figure 35. Gray-scale CCT's measured at V_s = 2 V of sample annealing behavior for Si(111) exposed to oxygen: (a) surface after 0.15 langmuir O_2 dose at 300 K, (b) different area of same sample after 60 s anneal at 625 K, and (c) different area after further 60 s anneal at 680 K (from ref 206).

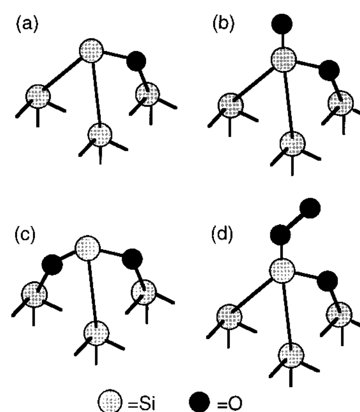

Figure 36. Structural model of oxygen reaction sites on Si(111)-(7×7).

Some differences in the experimental observations of the different groups have led to different interpretations of the atomic origins of these sites. Lyo et al. reported that the relative frequency of dark sites increased with exposure to either O_2 or N_2O (which dissociates to N_{2g} + O_{ads}). Lyo et al. concluded that the bright sites arise from the insertion of a single O atom into a Si−Si backbond, giving rise to the structure shown in Figure 36a. They also concluded that the "dark" sites arise from the interaction of an O_2 molecule which attaches to an adatom "dangling

bond" and subsequently dissociates, leaving one O atom attached to the dangling bond and a second O atom inserting into the Si−Si backbond, as in Figure 36b.

In contrast, Pelz and Koch reported imaging a single area of Si(111)-(7×7) at different oxygen exposures. At low exposure, the surface contained primarily "bright" sites. Continued imaging after this exposure reportedly produced no change in the STM images for periods as long as 1 h, indicating that the bright sites are reasonably stable at 300 K. When this same region was then re-exposed to oxygen and imaged again, it was found that the dark sites increased in frequency; however, the dark sites were all found at locations where previously there had been a bright site. Pelz and Koch therefore proposed a two-step oxidation mechanism. They proposed that the bright sites arise from an oxygen adatom which inserts into the backbond of a Si adatom (in agreement with Lyo et al.). However, they proposed that the dark sites arise from sites in which oxygen adatoms have inserted into two of the adatom backbonds, as in Figure 36c. Both groups reported that the bright sites show site-selective behavior, being found most frequently at the corner adatom sites; Lyo et al. proposed that the adsorption of O_2 passed through a negative-ion intermediate (O_2^-) and that the reaction at the corner adatom sites is most favored because these sites have high-density occupied states (or, in other words, electrons with the highest chemical potential). However, the nature of the dark sites has remained controversial. A recent investigation by Martel et al.,[217] however, showed that it is possible to restore a dark site back to a bright site by application of a voltage pulse. These authors argued that this indicates that the dark site entails adsorption of oxygen in molecular form and proposed that the "dark" sites contain an oxygen adatom in a backbond and, in addition, an oxygen molecule bonded onto the dangling bond, as shown in Figure 36d.

The interaction of O_2 with Si(111)-(7×7) at temperatures between 775 and 950 K has been investigated by Feltz et al.[218] and Seiple et al.[219] There is particular interest in this high-temperature regime because of the equilibrium between oxidation and etching of the surface via removal of volatile SiO products. Feltz et al. investigated the interaction at 950 K; at this temperature O_2 reacts to form SiO, which volatilizes, forming pits on flat terraces and etching the step edges. Whether the etching occurs at the steps or on the terraces was found to depend strongly on the density of defects (vacancies and antiphase boundaries) in the Si(111)-(7×7) reconstruction and on the separation between steps. At 950 K vacancies were found to be quite mobile, leading to the nucleation and growth of small pits into larger pits and the migration of some vacancies to step edges.

Many of the these same observations were confirmed by Seiple et al.,[219] who conducted experiments over a larger range of temperatures and pressures. At 775 K and exposure at low pressures (6×10^{-8} Torr), the surface appearance is similar to that observed after room-temperature dosing, except for the appearance of small pits on the surface, typically one double-layer deep, arising from the desorption of SiO. Surprisingly, at higher temperatures (875 K), the surface quality improves somewhat. Instead of the well-ordered (7×7) reconstruction, images in this temperature range typically show regions of (5×5) and/or (9×9) near the lower edge of steps. This in turn implies that the surface is being etched by a step-flow mechanism and that the regions exposed by the etching process do not have sufficient thermal energy to form the thermodynamically-stable (7×7) reconstruction but adopt any of a variety of DAS-type structures. By analyzing the number of pits as a function of the oxygen pressure during dosing at constant total exposure and constant sample temperature, it was shown that the nucleation of a pit is at least second order in oxygen pressure. It was proposed that the critical nucleation might involve interaction of diffusing oxygen-induced vacancies, the interaction of mobile surface oxygen as O_2 or SiO, or the interaction of Si vacancies with surface oxygen.

A final important conclusion from this work was the observation that there is a set of critical conditions defining whether silicon etches or oxidizes, depending on the ambient temperature and pressure. In the low-temperature regime, the STM results of Seiple et al.[219] suggest that the critical pressure required for oxidation is about 100 times higher than the value suggested by extrapolation of higher temperature data. Since the formation of small amounts of oxygen interfere with crystalline Si growth during CVD processes, this result suggests that the presence of small amounts of trace oxygen might be less problematic than originally thought.

g. Interaction of Ammonia with Si(111)

One of the earliest STM investigations of silicon reactivity focused on the interaction of ammonia (NH_3) with the Si(111)-(7×7) surface.[220−222] Earlier work using electron energy loss and photoemission spectroscopies had shown that NH_3 adsorbs dissociatively on Si(111), producing NH_{2ads} and H_{ads}.[223−225] STM images and tunneling spectroscopy measurements showed a striking spatial variation in chemical reactivity: Rest atom sites were the most reactive followed by the center adatom sites and then by the corner adatom sites. The variations in adatom reactivity were observed readily in STM images; reacted adatoms appeared dark at bias voltages of ca. 1 V and appeared bright at sample voltages of 3 V. Because the rest atoms are physically lower than the adatoms, the reactivity of rest atoms was most easily probed using tunneling spectroscopy measurements to look for the presence or absence of the characteristic spectroscopic feature at −0.8 V normally observed for the rest atoms on the clean surface.[195] These variations in chemical reactivity could be detected by STM imaging. After exposure to NH_3, STM images revealed that many of the adatoms appeared "dark" at STM bias voltages of ca. 1 V; however, the adatoms could be observed at larger sample bias voltages of ca. 3 V, demonstrating that the adatoms were still present but modified electronically by the NH_3 adsorption.

Since the rest atoms of the (7×7) structure are normally completely occupied, it is somewhat sur-

prising that these sites are reactive toward a molecule like ammonia, which has a lone electron pair. The reactivity of the rest atoms sites apparently arises from the ability of these atoms to transfer electrons back to the adatoms, which also leads to a shift in energy of the backbond state arising from the bonds between the adatoms and the substrate. The dissociative adsorption of NH_3 requires two sites, however, to accommodate the NH_{2ads} and H_{ads} fragments. While one fragment bonds at the rest atom site, the second fragment likely goes to the nearest available reactive site, which will be an adatom. Since each rest atom is surrounded by two "center" adatoms and only one "corner" adatom, one would expect a statistical 2:1 reactivity ratio between center adatoms and corner adatoms, while experimentally a ratio of larger than 4:1 was observed.[221] The unusually high reactivity of the center adatoms was attributed to higher strain produced in the DAS dimers upon reaction of a corner adatom. Because NH_{2ads} and H_{ads} both reduce the density of electronic states near the Fermi energy, it was not possible to discriminate between these two fragments in the STM images, and it was not possible to determine if either of the two fragments exhibited a preference for a particular reactive site.

h. Interaction of Decaborane with Si(111)

The interaction of decaborane with Si(111) is of interest since boron is a p-type dopant in Si and also because the reconstructions produced by boron on Si(111) have interesting structural and electronic properties. As on the Si(001) surface,[160,164−168] boron on Si(111) can order into "δ-doped" layers that are of great interest for potential microelectronics applications.[226]

The interaction of $B_{10}H_{14}$ with Si(111) was investigated by Lyo et al.[227,228] At room temperature, the decaborane molecule adsorbs on the Si(111) surface and appears as a round protrusion. Decaborane exhibits some selectivity for specific Si(111) surface sites. In Figure 37, it can be seen that the round protrusion is most often centered directly over the "center" adatoms of the Si(111)-(7×7) structure, while the $B_{10}H_{14}$ molecules avoid covering the corner hole as well as the adatoms immediately adjacent to it. Electron energy loss spectra by Chen et al.[229] also show that adsorption of decaborane occurs molecularly, as evidenced by the absence of Si−H stretching vibrations on $B_{10}H_{14}$-exposed Si(111) surfaces. TPD and EELS spectra show that dissociation of decaborane is complete by 900 K. However, LEED studies showed that the resulting surface was disordered. Ordering of the boron atoms into a $(\sqrt{3}\times\sqrt{3})R30°$ structure occurred only after the sample was annealed for an extended period of time. STM images of the surfaces exposed to small amounts of decaborane (Figure 38a) show a mixed phase in which the (7×7) reconstruction is eliminated and replaced by a $(\sqrt{3}\times\sqrt{3})R30°$ structure but with the heights of the unit cells varying randomly due to random lateral distributions of the boron atoms. At higher decaborane exposures and after higher annealing temperature (Figure 38b), a well-ordered $(\sqrt{3}\times\sqrt{3})R30°$ reconstruction is observed.

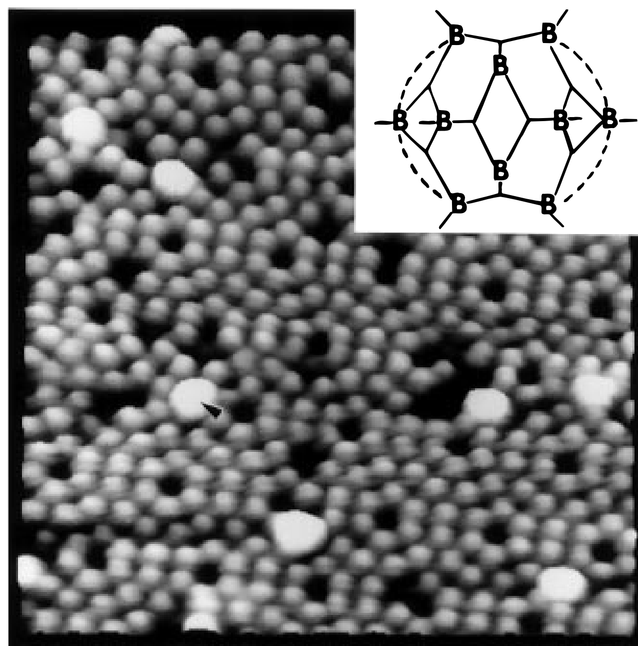

Figure 37. STM topograph of Si(111)-(7×7) surface exposed to 0.2 langmuir of decaborane (sample bias = 2 V) (from ref 228).

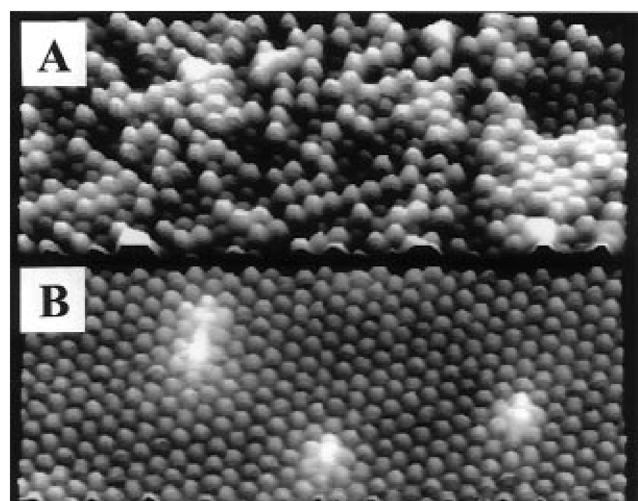

Figure 38. STM topograph of surfaces produced by exposing Si(111)-(7×7) to (A) 0.4 langmuir of decaborane at 300 K and briefly annealing to 1075 K and (B) 1 langmuir of decaborane and annealing to 1275 K (from ref 228).

While in most cases the surface chemistry is associated with species adsorbed on top of the original surface, in the case of boron this is not true. In the gas phase, compounds in which boron has a coordination number of 3 are typically planar (for example, BCl_3). As a result, it is difficult for boron to adopt the proper tetrahedral coordination to terminate the dangling bonds of either the adatoms or a bulklike Si(111) surface. As a B^- anion, however, boron will tend toward sp^3 hybridization and will favor a position of tetrahedral coordination. This favorable situation is readily achieved by a migration of boron to a substitutional site known as the "T4" site, as depicted in Figure 39. In the T4 site, the boron atom is tetrahedrally coordinated. The negative charge can be readily drawn from the Si adatom directly above it. This configuration of boron directly beneath

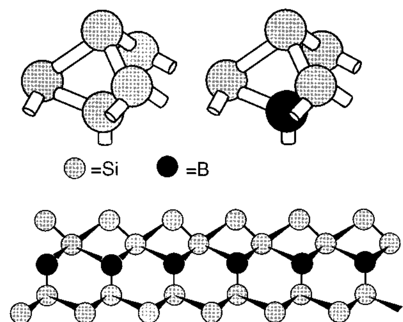

Figure 39. Structural model of boron-induced reconstruction on Si(111).

a Si adatom is essentially a charge-transfer complex in which the electron normally present in the Si adatom "dangling bond" is transferred to the boron atom. In this configuration, it appears that the removal of the surface dangling bond through this charge-transfer process again obviates the need for the alternating stacking fault structure. As a result, the surface adopts a simple $(\sqrt{3}\times\sqrt{3})R30°$ structure which is shown in Figures 38 and 39. This same structure has been produced by several methods. Avouris et al. used thermal decomposition of decaborane, while Bedrossian and co-workers prepared the same surface (with identical characteristics in the STM images) both by annealing highly-boron-doped wafers and by sputtering boron onto the surface from a separate source.[230,231] The formation of the identical structure from three different preparation techniques suggests that this boron-induced structure is very stable thermodynamically; moreover, its creation by diffusion processes in highly-doped wafers indicates that boron atoms in this T4 structure are more stable than boron atoms on substitutional sites in the bulk. This might arise from the ability to accommodate some of the lattice strain at the free surface that cannot be otherwise accommodated in the bulk. The T4 geometry inferred from the STM measurements is fully confirmed by X-ray diffraction measurements.[232]

One of the most interesting aspects of the boron-induced reconstruction is that, like the Si(001) analog, it is possible to deposit Si on the boron layers to achieve "δ-doped" Si layers. Headrick et al. showed that when Si is deposited on the $(\sqrt{3}\times\sqrt{3})R30°$ B/Si-(111) reconstruction, the Si which grows is crystalline, but its crystallographic orientation is rotated by 180° with respect to the underlying Si substrate.[167] This corresponds to a twin boundary that is equivalent to a monolayer of wurtzite structure instead of diamond structure Si. This stacking fault persists even after annealing to temperatures where the boron diffuses away from the T4 site into the bulk crystal lattice. Electrical conductivity measurements made after deposition of amorphous Si on the $\sqrt{3}$B/Si(111) surface show that not only are the boron atoms electrically active (as expected from their tetrahedral location) but also that the mobility of the holes produced is higher than that of bulk Si.[171] As with boron on Si(001), the δ-doped layer formation on Si(111) provides a possible low-temperature route to very high dopant concentrations while maintaining high electrical quality.

i. Interaction of Acetylene with Si(111)-(7×7)

As in the case of Si(111), the primary motivation for investigating hydrocarbon interactions with silicon surfaces is for the growth of silicon carbide and/or diamond.[233] A strongly-site-selective reactivity was observed, with the faulted half of the unit cell being about 3 times more reactive than the unfaulted half and center adatoms about 2 times as reactive as corner adatoms.[233] Yoshinobu et al. observed that no more than three adatoms within a given unit cell would usually react.[233] Previous electron energy loss spectroscopy data[234] indicated that the acetylene was not bonded through a π bond but most likely formed two new σ bonds (a "di-σ" configuration), in a manner qualitatively similar to its behavior on Si(001) discussed earlier in this article. This configuration has also been predicted theoretically.[235,236] Although the Si(111)-(7×7) reconstruction has a rich variety of possible adsorption sites, many of them are separated by distances which are much longer than typical C−C bond lengths of 1.2−1.5 Å and therefore would most likely involve a very high energy transition state to adsorption. For example, adatoms on the Si(111)-(7×7) surface are separated by 7.7 Å. The closest reactive sites on Si(111)-(7×7) are one rest atom and an adjacent adatom, separated horizontally by about 4.3 Å. Yoshinobu et al. proposed that the acetylene molecule was di-σ bonded on one rest atom and one adatom. Within this model, the relative reactivities of center and corner adatoms can be accounted for solely on the site statistics: Each corner adatom is surrounded by one rest atom (not including the dangling bond in the corner hole), while center adatoms are surrounded by two. Therefore, a ratio of about 2:1 would be anticipated for the relative reactivities of corner and center adatoms, in good agreement with the experimental observations. The preferential reactivity of the faulted vs unfaulted halves of the unit cell was again attributed to the known differences in electronic structure between these two.[195]

IV. Summary and Conclusions

With the above set of experimental observations, it is possible to begin making some generalizations about the chemistry of silicon surfaces. One important observation is that the surface reconstructions clearly play an important role in the overall chemistry of the surface. The same factors which are responsible for creating the reconstructions, namely, that the Si surface energy is minimized when as many Si atoms as possible have achieved 4-fold coordination, are also ultimately responsible for most of the variations in chemical reactivity. The atoms at surfaces are also highly strained, and many of the observations reported above can be described in terms of a competition between optimization of overall coordination and the minimization of strain resulting from nonideal bond lengths or bond angles.

The comparatively-simple reconstruction of the Si-(001) surface belies the overall complexity of its reactivity. For simple adsorbates such as H, Cl, and Br, it is clear that the chemistry at low coverages can be understood in terms of the termination of the

dimer dangling bonds. This leads to a preferential pairing of H, Cl, and Br into monohydride, monochloride, and monobromide structures, respectively. At higher coverages, etching processes are directly observed via insertion into Si−Si bonds. Likewise, the chemistry of disilane and germane on Si(001) can be largely understood on these same principles. The absence of any discrete SiH adspecies, for example, is a direct result of the inability of such a species to bond to the Si(001) surface while still maintaining 4-fold coordination.

The chemistry of molecules such as phosphine and diborane is intrinsically more complicated because the phosphorus and boron not only adsorb on the surface but also can substitute directly for Si in the crystal lattice. Because these atoms have a different "size" than the Si atom they replace, substitution is accompanied by lattice strain. In both these cases, STM investigations probing the spatial distribution of reactants have provided new insight into the surface structures, while the combination of STM with infrared spectroscopy has provided an understanding of the role these atoms play in affecting other chemical reactions occurring on the surface.

Although not as relevant for technological applications, the Si(111)-(7×7) surface provides a rich variety of reactive surface sites and will no doubt be a model system for years to come. With the exception of atomic hydrogen (which has a reaction probability of essentially 1), all other chemical systems (SiH_4, GeH_4, Ge_2H_6, O_2, H_2O, etc.) show a preference for reacting at specific sites within the (7×7) unit cell. In some cases (such as oxygen) the reaction probabilities can be understood based on the local electronic state densities of the different adatom sites: Corner adatoms in the faulted half of the unit cell have the highest state density and act as the most nucleophilic reaction site. Yet, other reactions (such as SiH_4) appear to be controlled by the nature of the dangling bonds on the rest atom and "corner hole" sites.

The level of complexity exhibited both in the structure and in the reaction chemistry of silicon surfaces is almost certainly far beyond what anyone expected before the invention of the scanning tunneling microscope provided the ability to observe surfaces and their reactions in real space (and, in some cases, real time). To date, most studies have focused on the simplest chemical systems because of their general importance and also because of the unexpected complexity of even these systems. A general difficulty in applying STM to investigate more complicated chemical reactions is the general problem of identification of species at an atomic level. While coordination-based approaches to identifying surface species have been shown to work for several chemical systems such as SiH_x and $SiCl_x$ species, these methods are not as easily extendable to other chemical systems and assume that the overall coordination number for a given element is known. As STM begins to mature, it is increasingly being integrated with other chemical analysis techniques, such as infrared spectroscopy, to provide both atomic-level spatial analysis and high-quality chemical analysis.

Acknowledgments

The authors would like to express their appreciation for the National Science Foundation, the U.S. Office of Naval Research, and the Camille and Henry Dreyfus Foundation for support of their research in the STM field.

References

(1) Bardeen, J.; Brattain, W. H. *Phys. Rev. Lett.* **1948**, *74*, 230.
(2) Binnig, G.; Rohrer, H.; Gerber, C.; Weibel, E. *Phys. Rev. Lett.* **1983**, *50*, 120.
(3) Binnig, G.; Rohrer, H. *Helv. Phys. Acta* **1982**, *55*, 726.
(4) Bardeen, J. *Phys. Rev. Lett.* **1961**, *6*, 57.
(5) Tersoff, J.; Hamann, D. R. *Phys. Rev. Lett.* **1983**, *50*, 1998.
(6) Tersoff, J.; Hamann, D. R. *Phys. Rev. B* **1985**, *31*, 805.
(7) Tersoff, J. In *Scanning Tunneling Microscopy and Related Methods*; Behm, R. J., Garcia, N., Rohrer, H., Eds.; Kluwer: Dordrecht, Boston, New York, 1990; Vol. 184, pp 77.
(8) Waltenburg, H. N.; Yates, J. T., Jr. *Chem. Rev.* **1995**, *95*, 1589.
(9) Schlier, R. E.; Farnsworth, H. E. *J. Chem. Phys.* **1959**, *30*, 917.
(10) Seiwatz, R. *Surf. Sci.* **1964**, *2*, 473.
(11) Phillips, J. C. *Surf. Sci.* **1973**, *40*, 459.
(12) Poppendieck, T. D.; Gnoc, T. C.; Webb, M. B. *Surf. Sci.* **1974**, *43*, 647.
(13) Appelbaum, J. A.; Baraff, G. A.; Hamann, D. R. *Phys. Rev. B* **1976**, *14*, 588.
(14) Appelbaum, J. A.; Baraff, G. A.; Hamann, D. R. *Phys. Rev. Lett.* **1975**, *35*, 729.
(15) Appelbaum, J. A.; Baraff, G.; Hamann, D. R.; Hagstrom, H. D.; Sakurai, T. *Surf. Sci.* **1978**, *70*, 654.
(16) Chadi, D. J. *Phys. Rev. Lett.* **1979**, *43*, 43.
(17) Hamers, R. J.; Tromp, R. M.; Demuth, J. E. *Phys. Rev. B* **1986**, *34*, 5343.
(18) Hamers, R. J.; Tromp, R. M.; Demuth, J. E. *Surf. Sci.* **1987**, *181*, 246.
(19) Tromp, R. M.; Hamers, R. J.; Demuth, J. E. *Phys. Rev. Lett.* **1985**, *55*, 1303.
(20) Appelbaum, J. A.; Baraff, G. A.; Hamann, D. R. *Phys. Rev. B* **1977**, *15*, 2408.
(21) Hamers, R. J.; Avouris, P.; Bozso, F. *Phys. Rev. Lett.* **1987**, *59*, 2071.
(22) D'Evelyn, M. P.; Yang, Y.; Sutcu, L. *J. Chem. Phys.* **1992**, *96*, 852.
(23) Nachtigall, P.; Jordan, K. D. *J. Chem. Phys.* **1995**, *102*, in press.
(24) Nachtigall, P.; Jordan, K. D.; Sosa, C. *J. Chem. Phys.* **1994**, *101*, 8073.
(25) Wu, C. J.; Carter, E. A. *Phys. Rev. B* **1992**, *46*, 4651.
(26) Wu, C. J.; Carter, E. A. *Chem. Phys. Lett.* **1991**, *185*, 172.
(27) Hofer, U.; Li, L.; Heinz, T. F. *Phys. Rev. B* **1992**, *45*, 9485.
(28) Gates, S. M.; Greenlief, C. M.; Beach, D. B. *J. Chem. Phys.* **1990**, *93*, 7493.
(29) Walsh, R. *Acc. Chem. Res.* **1990**, *14*, 246.
(30) Tabata, T.; Aruga, T.; Murata, Y. *Surf. Sci.* **1986**, *179*, L63.
(31) Wolkow, R. A. *Phys. Rev. Lett.* **1992**, *68*, 2636.
(32) Wang, Y.; Bronikowski, M. J.; Hamers, R. J. *Surf. Sci.* **1994**, *311*, 64.
(33) Sakurai, T.; Hagstrum, H. D. *Phys. Rev. B* **1976**, *14*, 1593.
(34) Sinniah, K.; Sherman, M. G.; Lewis, L. B.; Weinberg, W. H.; Yates, J. T., Jr.; Janda, K. C. *Phys. Rev. Lett.* **1989**, *62*, 567.
(35) Sinniah, K.; Sherman, M. G.; Lewis, L.; Weinberg, W. H.; Yates, J. T., Jr.; Janda, K. C. *J. Chem. Phys.* **1990**, *92*, 5700.
(36) Ibach, H.; Rowe, J. E. *Surf. Sci.* **1974**, *43*, 481.
(37) Gates, S. M.; Kunz, R. R.; Greenlief, C. M. *Surf. Sci.* **1989**, *207*, 364.
(38) Schaefer, J. A.; Anderson, F.; Anderson, J. R.; Lapeyre, G. J.; Gopel, W. *Surf. Sci.* **1984**, *140*, 207.
(39) Ciraci, S.; Butz, R.; Oellig, E. M.; Wagner, H. *Phys. Rev. B* **1984**, *30*, 711.
(40) Jasinski, J. M.; Gates, S. M. *Acc. Chem. Res.* **1991**, *24*, 9.
(41) Jasinski, J. M.; Meyerson, B. S.; Scott, B. A. *Annu. Rev. Phys. Chem.* **1987**, *38*, 109.
(42) Law, J. T. *J. Phys. Chem.* **1959**, *30*, 1568.
(43) Johansson, L. S. O.; Uhrberg, R. I. G.; Hansson, G. V. *Phys. Rev. B* **1988**, *38*, 13490.
(44) Johansson, L. S. O.; Reihl, B. *Phys. Rev. Lett.* **1991**, *67*, 2191.
(45) Hamers, R. J.; Avouris, P.; Bozso, F. *J. Vac. Sci. Technol. A* **1988**, *6*, 508.
(46) Boland, J. J. *Phys. Rev. B* **1991**, *44*, 1383.
(47) Boland, J. J. *Phys. Rev. Lett.* **1991**, *67*, 1539.
(48) Boland, J. J. *Phys. Rev. Lett.* **1990**, *65*, 3325.
(49) Boland, J. J. *Science* **1992**, *255*, 186.
(50) Wang, Y.; Bronikowski, M. J.; Hamers, R. J. *J. Vac. Sci. Technol. A* **1994**, *12*, 2051.
(51) Boland, J. J. *J. Phys. Chem.* **1991**, *95*, 1521.
(52) Naitoh, M.; Morioka, H.; Shoji, F. *Surf. Sci.* **1993**, *297*, 135.
(53) Koleske, D. D.; Gates, S. M.; Schultz, J. A. *J. Chem. Phys.* **1993**, *99*, 5619.

(54) Shen, T. C.; et al. *Science* **1995**, *268*, 1590.
(55) Shen, T. C.; Wang, C.; Lyding, J.; Tucker, J. R. *Appl. Phys. Lett.* **1995**, *66*, 976.
(56) Gates, S. M. *Surf. Sci.* **1988**, *195*, 307.
(57) Gates, S. M.; Greenlief, C. M.; Kulkarni, S. K.; Sawin, H. H. *J. Vac. Sci. Technol.* **1990**, *A8*, 2965.
(58) Gates, S. M.; Chiang, C. M. *Chem. Phys. Lett.* **1991**, *184*, 448.
(59) Gates, S. M.; Kulkarni, S. K. *Appl. Phys. Lett.* **1991**, *58*, 2963.
(60) Wise, M. L.; Koehler, B. G.; Gupta, P.; Coon, P. A.; George, S. M. *Surf. Sci.* **1991**, *258*, 166.
(61) Schulze, G.; Henzler, M. *Surf. Sci.* **1983**, *124*, 336.
(62) Redhead, P. A. *Vacuum* **1962**, 203.
(63) Flowers, M. C.; Jonathan, N. B.; Liu, Y.; Morris, A. *J. Chem. Phys.* **1993**, *99*, 7038.
(64) Kolasinski, K. W.; Shane, S. F.; Zare, R. N. *J. Chem. Phys.* **1992**, *96*, 3995.
(65) Kolasinski, K. W.; Shane, S. F.; Zare, R. N. *J. Chem. Phys.* **1991**, *95*, 5482.
(66) Jing, Z.; Whitten, J. L. *J. Chem. Phys.* **1993**, *98*, 7466.
(67) Cheng, C. C.; Yates, J. T., Jr. *Phys. Rev. B* **1991**, *43*, 4041.
(68) Chabal, Y. J.; Raghavachari, K. *Phys. Rev. Lett.* **1985**, *54*, 1055.
(69) Boland, J. J. *Surf. Sci.* **1992**, *261*, 17.
(70) Bozso, F.; Avouris, P. *Phys. Rev. B* **1988**, *38*, 3943.
(71) Lubben, D.; Tsu, R.; Bramblett, T. R.; Greene, J. E. *J. Vac. Sci. Technol. A* **1991**, *9*, 3003.
(72) Wu, Y. M.; Baker, J.; Hamilton, P.; Nix, R. M. *Surf. Sci.* **1993**, *295*, 133.
(73) Isobe, C.; Cho, H.-C.; Crowell, J. E. *Surf. Sci.* **1993**, *295*, 99.
(74) Suda, Y.; Lubben, D.; Motooka, T.; Greene, J. E. *J. Vac. Sci. Technol.* **1990**, *8*, 61.
(75) Gates, S. M. *J. Cryst. Growth* **1992**, *120*, 269.
(76) Gates, S. M.; Kulkarni, S. K. *Appl. Phys. Lett.* **1992**, *60*, 53.
(77) Hamers, R. J.; Shan, J.; Wang, Y. *Appl. Surf. Sci.* **1995**, in press.
(78) Gates, S. M.; Scott, B. A.; Beach, D. B.; Imbihl, R.; Demuth, J. E. *J. Vac. Sci. Technol.* **1987**, *A5*, 628.
(79) Gates, S. M. *J. Phys. Chem.* **1992**, *96*, 10439.
(80) Bronikowski, M. J.; Wang, Y.; McEllistrem, M. T.; Chen, D.; Hamers, R. J. *Surf. Sci.* **1993**, *298,* 50.
(81) Bronikowski, M. J.; Wang, Y.; Hamers, R. J. *Phys. Rev. B* **1993**, *48,* 12361.
(82) Lin, D. S.; Hirschorn, E. S.; Chiang, T. C.; Tsu, R.; Lubben, D.; Greene, J. E. *Phys. Rev. B* **1992**, *45*, 3494.
(83) Barin, I. *Thermochemical Data of Pure Substances*; VCH Publishers: Weinheim, 1989.
(84) Suntola, T. *Mater. Sci. Rep.* **1989**, *4*, 261.
(85) Thornton, G.; Wincott, P. L.; BcGrath, R.; McGovern, I. T.; Quinn, F. M.; Normal, D.; Vvedensky, D. D. *Surf. Sci.* **1989**, *211/212*, 959.
(86) Szabo, Z.; Farral, P. D.; Engel, T. *Surf. Sci.* **1994**, *312*, 284.
(87) Bennett, S. L.; Greenwood, C. L.; Williams, E. M. *Surf. Sci.* **1993**, *290*, 267.
(88) Gao, Q.; Cheng, C. C.; Chen, P. J.; Choyke, W. J.; Yates, J. T., Jr. *J. Chem. Phys.* **1993**, *98*, 8308.
(89) Cheng, C. C.; Gao, Q.; Choyke, W. J.; Yates, J. T., Jr. *Phys. Rev. B* **1992**, *46*, 810.
(90) Sterratt, D.; Greenwood, C. L.; Williams, E. M.; Muryn, C. A.; Wincott, P. L.; Thornton, G.; Roman, E. *Surf. Sci.* **1994**, *307*, 269.
(91) Bronikowski, M. J.; Hamers, R. J. *J. Vac. Sci. Technol. A* **1995**, *13*, 777.
(92) Boland, J. J. *Science* **1993**, *262*, 1703.
(93) Chander, M.; Li, Y. Z.; Patrin, J. C.; Weaver, J. H. *Phys. Rev. B* **1993**, *47*, 13035.
(94) Chander, M.; Li, Y. Z.; Rioux, D.; Weaver, J. H. *Phys. Rev. Lett.* **1993**, *71*, 4154.
(95) Rioux, D.; Chander, M.; Li, Y. Z.; Weaver, J. H. *Phys. Rev. B* **1994**, *49*, 11071.
(96) *Physics and Chemistry of SiO2 and the Si−SiO2 Interface*; Helms, C. R., Deal, B. E., Eds.; Plenum Press: New York, 1988.
(97) Deal, B. E.; Grove, A. S. *J. Appl. Phys.* **1965**, *36*, 3770.
(98) Froitzheim, H. In *The Chemical Physics of Solid Surfaces and Heterogeneous Catalysis, vol 5: Surface Properties of Electronic Materials*; King, D. A., Woodruff, D. P., Eds.; Elsevier: Amsterdam, 1988.
(99) Cahill, D. G.; Avouris, P. *Appl. Phys. Lett.* **1992**, *60*, 326.
(100) Avouris, P.; Cahill, D. G. *Ultramicroscopy* **1992**, *42−44*, 838.
(101) Johnson, K. E.; Wu, P. K.; Sander, M.; Engel, T. *Surf. Sci.* **1993**, *290*, 213.
(102) Ralls, K. S.; Skocpol, W. J.; Jackel, L. D.; Howard, R. E.; Fetter, L. A.; Epworth, R. W.; Tennant, D. M. *Phys. Rev. Lett.* **1984**, *52*, 228.
(103) Uren, M. J.; Day, D. J.; Kirton, M. J. *Appl. Phys. Lett.* **1985**, *47*, 1195.
(104) Koch, R. H.; Hamers, R. J. *Surf. Sci.* **1987**, *181*, 333.
(105) Hamers, R. J.; Koch, R. H. In *Physics and Chemistry of SiO2 and the Si−SiO2 Interface*; Helms, C. R., Deal, B. A., Eds.; Plenum: New York, 1988.
(106) D'Evelyn, M. P.; Nelson, M. M.; Engel, T. *Surf. Sci.* **1987**, *186*, 75.
(107) Gupta, P.; Mak, C. H.; Coon, P. A.; George, S. M. *Phys. Rev. B* **1989**, *40*, 7739.
(108) Hamers, R. J.; Köhler, U. K. *J. Vac. Sci. Technol. A* **1989**, *7*, 2854.
(109) Udagawa, M.; Umetani, Y.; Tanaka, H.; Itoh, M.; Uchiyama, T.; Watanabe, Y.; Yokotusuka, T.; Sumita, I. *Ultramicroscopy* **1992**, *42−44*, 946.
(110) Fahey, P. M.; Griffin, P. B.; Plummer, J. D. *Rev. Mod. Phys.* **1989**, *61*, 289.
(111) Hu, S. M. *J. Appl. Phys.* **1974**, *45*, 1567.
(112) Incoccia, L.; Balerna, A.; Cramm, S.; Kunz, C.; Senf, F.; Storjohann, I. *Surf. Sci.* **1987**, *189/190*, 453.
(113) Liehr, M.; Lewis, J. E.; Rubloff, G. W. *J. Vac. Sci. Technol. A* **1987**, *8*, 1559.
(114) Rubloff, G. W. *J. Vac. Sci. Technol. A* **1990**, *8*, 1857.
(115) Sun, Y.-K.; Bonser, D. J.; Engel, T. *J. Vac. Sci. Technol. A* **1992**, *10*, 2314.
(116) Sun, Y.-K.; Bonser, D. J.; Engel, T. *Phys. Rev. B* **1991**, *43*, 14309.
(117) Kobayashi, Y.; Sugii, K. *J. Vac. Sci. Technol. A* **1992**, *10*, 2308.
(118) Johnson, K. E.; Engel, T. *Phys. Rev. Lett.* **1992**, *69*, 339.
(119) Srivastava, D.; Garrison, B. J. *J. Chem. Phys.* **1991**, *95*, 6885.
(120) Zhang, Z.; Lu, Y.; Metiu, H. *Surf. Sci. Lett.* **1991**, *248*, L250.
(121) Thiel, P. A.; Madey, T. E. *Surf. Sci. Rep.* **1987**, *7*, 211.
(122) Fujiwara, K. *Surf. Sci.* **1981**, *108*, 124.
(123) Schmeisser, D.; Himpsel, F. J.; Hollinger, G. *Phys. Rev. B* **1983**, *27*, 7813.
(124) Andersohn, L.; Kohler, U. *Surf. Sci.* **1993**, *284*, 77.
(125) Chander, M.; Li, Y. Z.; Patrin, J. C.; Weaver, J. H. *Phys. Rev. B* **1993**, *48*.
(126) Ibach, H.; Wagner, H.; Bruchmann, D. *Solid State Commun.* **1982**, *42*, 457.
(127) Chabal, Y. J. *Phys. Rev. B* **1984**, *29*, 3677.
(128) Chabal, Y. J.; Christmann, S. B. *Phys. Rev. B* **1984**, *29*, 6974.
(129) Farrow, R. F. C. *J. Electrochem. Soc.* **1974**, *120*, 106.
(130) Chang, C. A. *J. Electrochem. Soc.* **1976**, *123*, 1245.
(131) Meyerson, B. S.; Olbricht, W. *J. Electrochem. Soc.* **1984**, *131*, 2361.
(132) Copel, M. *Phys. Rev. B* **1990**, *42*, 11682.
(133) Copel, M.; Reuter, M.; Kaxiras, E.; Tromp, R. M. *Phys. Rev. Lett.* **1989**, *63*, 632.
(134) Yu, M. L.; Meyerson, B. S. *J. Vac. Sci. Technol. A* **1984**, *2*, 446.
(135) Yu, M. L.; Vitkavage, D. J.; Meyerson, B. S. *J. Appl. Phys.* **1986**, *59*, 4032.
(136) Colaianni, M. L.; Chen, P. J.; Yates, J. T., Jr. *J. Vac. Sci. Technol. A* **1994**, *12*, 2995.
(137) Wang, Y.; Bronikowski, M. J.; Hamers, R. J. *J. Phys. Chem.* **1994**, *98*, 5966.
(138) Wang, Y.; Chen, X.; Hamers, R. J. *Phys. Rev. B* **1994**, *50*, 4534.
(139) Shan, J.; Wang, Y.; Hamers, R. J. *J. Phys. Chem.* **1996**, *100,* 4961.
(140) Cao, P. L.; Lee, L. Q.; Dai, J. J.; Zhou, R. H. *J. Phys. Condens. Matter* **1994**, *6*, 6103.
(141) Kipp, L.; Bringans, R. D.; Biegelsen, D. K.; Northrup, J. E.; Garcia, A.; Swartz, L. E. *Phys. Rev. B* **1995**, *52*, 5843.
(142) Chabal, Y. J.; Higashi, G. S.; Christman, S. B. *Phys. Rev. B* **1983**, *28*, 4472.
(143) Chabal, Y. J.; Raghavachari, K. *Phys. Rev. Lett.* **1984**, *53*, 282.
(144) Wang, W.-C.; Denton, J. P.; Neudeck, G. W. *J. Vac. Sci. Technol. B* **1993**, *11*, 117.
(145) Madsen, L. D.; Weaver, L. *J. Electrochem. Soc.* **1990**, *137*, 2246.
(146) Kuhne, H.; Puk, P.; Gericke, M.; Bertoldi, W. *Cryst. Res. Technol.* **1990**, *25*, 497.
(147) Jang, S.-M. *Appl. Phys. Lett.* **1993**, *63*, 1675.
(148) Greve, D. W.; Racanelli, M. *J. Electrochem. Soc.* **1991**, *138*, 1744.
(149) Yoo, D. S.; Suemitsu, M.; Miyamoto, N. *J. Appl. Phys.* **1995**, *78*, 4988.
(150) Gates, S. M.; Greenlief, C. M.; Beach, D. B.; Holbert, P. A. *J. Chem. Phys.* **1990**, *92*, 3144.
(151) Bozso, F.; Avouris, P. *Phys. Rev. Lett.* **1986**, *57*, 1185.
(152) Peden, C. H. F.; Rogers, J. W.; Kidd, K. B.; Tsang, K. L.; Shinn, N. D. *Mater. Res. Soc. Symp. Proc.* **1991**, *204*, 521.
(153) Fujisawa, M.; Taguchi, Y.; Kuwahara, Y.; Onchi, M.; Nishijima, M. *Phys. Rev. B* **1989**, *39*, 12918.
(154) Chen, P. J.; Colaianni, M. L.; Yates, J. T., Jr. *Surf. Sci.* **1992**, *274*, L605.
(155) Bischoff, J. L.; Lutz, F.; Bolmont, D.; Kubler, L. *Surf. Sci.* **1991**, *251−252*, 170.
(156) Larsson, C. S.; Flodstrom, A. S. *Surf. Sci.* **1991**, *241*, 353.
(157) Dresser, M. J.; Taylor, P. A.; Wallace, R. M.; Choyke, W. J.; Yates, J. T., Jr. *Surf. Sci.* **1989**, *218*, 75.
(158) Dufour, G.; Rochet, F.; Roulet, H.; Sirotti, F. *Surf. Sci.* **1994**, *304*, 33.
(159) Lu, Q.; Brambletrt, T. R.; Lee, N.-E.; Hasan, M.-A.; Karasawa, T.; Greene, J. E. *J. Appl. Phys.* **1995**, *77*, 3067.
(160) Meyerson, B. S.; LeGoues, F. K.; Nguyen, T. N.; Harame, D. L. *Appl. Phys. Lett.* **1987**, *50*, 113.
(161) Hajjar, J.-J.; Reif, R. *J. Electrochem. Soc.* **1990**, *137*, 2888.
(162) Bramblett, T. R.; Lu, Q.; Karasawa, T.; Hasan, M.-A.; Jo, S. K.; Greene, J. E. *J. Appl. Phys.* **1994**, *76*, 1884.

(163) Klatt, J.; Kruger, D.; Bugiel, E.; Osten, H. J. *Appl. Phys. Lett.* **1994**, *64*, 360.
(164) Headrick, R. L.; Weir, B. E.; Levi, A. F. J.; Freer, B.; Bevk, J.; Feldman, L. C. *J. Vac. Sci. Technol. A* **1991**, *9*, 2269.
(165) Gossmann, H.-J.; Schubert, E. F. *CRC Crit. Rev. Mater. Sci.* **1993**, *18*, 1.
(166) Cao, R.; Yang, X.; Pianetta, P. *J. Vac. Sci. Technol. B* **1993**, *11*, 1455.
(167) Headrick, R. L.; Weir, B. E.; Bevk, J.; Freer, B. S.; Eaglesham, D. J.; Feldman, L. C. *Phys. Rev. Lett.* **1990**, *65*, 1128.
(168) Weir, B. E.; Feldman, L. C.; Monroe, D.; Gossmann, H.-J.; Headrich, R. L.; Hart, T. R. *Appl. Phys. Lett.* **1994**, *65*, 737.
(169) Wang, Y.; Shan, J.; Hamers, R. J. *J. Chem. Phys.* **1996**, submitted for publication.
(170) Wang, Y.; Hamers, R. J.; Kaxiras, E. *Phys. Rev. Lett.* **1995**, *74*, 403.
(171) Headrick, R. L.; Lefi, A. F. J.; Luftman, H. S.; Kovalchick, J.; Feldman, L. C. *Phys. Rev. B* **1991**, *43*, 14711.
(172) Wang, Y.; Shan, J.; Hamers, R. J. *J. Vac. Sci. Technol. B* **1996**, in press.
(173) Wang, Y.; Hamers, R. J. *J. Vac. Sci. Technol. A* **1995**, *13*, 1431.
(174) Wang, Y.; Hamers, R. J. *Appl. Phys. Lett.* **1995**, *66*, 2057.
(175) Forster, A.; Luth, H. *J. Vac. Sci. Technol. B* **1989**, *7*, 720.
(176) Luth, H. *J. Vac. Sci. Technol. A* **1989**, *7*, 696.
(177) Gow, T. R.; Lin, R.; Masel, R. I. *J. Cryst. Growth* **1990**, *106*, 577.
(178) Kuech, T. F. *Proc. IEEE* **1992**, *80*, 1609.
(179) Bronikowski, M. J.; Hamers, R. J. *Surf. Sci.* **1995**, in press.
(180) Baski, A. A.; Nogami, J.; Quate, C. F. *J. Vac. Sci. Technol. A* **1990**, *8*, 245.
(181) Northrup, J. E.; Schabel, M. C.; Karlsson, C. J.; Uhrberg, R. I. G. *Phys. Rev. B* **1991**, *44*, 13799.
(182) Nogami, J.; Baski, A. A.; Quate, C. F. *J. Vac. Sci. Technol. A* **1990**, *8*, 3520.
(183) Nogami, J.; Park, S.; Quate, C. F. *Appl. Phys. Lett.* **1988**, *53*, 2086.
(184) Bourguignon, B.; Carleton, K. L.; Leone, S. R. *Surf. Sci.* **1988**, *204*, 455.
(185) Colaianni, M. L.; Chen, P. J.; Gutleben, H.; Yates, J. T., Jr. *Chem. Phys. Lett.* **1992**, *191*, 561.
(186) Gutleben, H.; Lucas, S. R.; Cheng, C. C.; Choyke, W. J.; Yates, J. T., Jr. *Surf. Sci.* **1991**, *257*, 146.
(187) Bozack, M. J.; Taylor, P. A.; Choyke, W. J.; Yates, J. T., Jr. *Surf. Sci.* **1986**, *177*, L933.
(188) Yoshinobu, J.; Tsuda, H.; Onchi, M.; Nishijima, M. *J. Chem. Phys.* **1987**, *87*, 7332.
(189) Nishijima, M.; Yoshinobu, J.; Tsuda, H.; Onchi, M. *Surf. Sci.* **1987**, *192*, 383.
(190) Cheng, C. C.; Wallace, R. M.; Taylor, P. A.; Choyke, W. J.; Yates, J. T., Jr. *J. Appl. Phys.* **1990**, *67*, 3693.
(191) Taylor, P. A.; Wallace, R. M.; Cheng, C. C.; Weinberg, W. H.; Dresser, M. J.; Choyke, W. J.; Yates, J. T., Jr. *J. Am. Chem. Soc.* **1992**, *114*, 6754.
(192) Mayne, A. J.; Cataldi, T. R. I.; Knall, J.; Avery, A. R.; Jones, T. S.; Pinheiro, L.; Hill, H. A. O.; Briggs, G. A. D.; Pethica, J. B.; Weinberg, W. H. *Faraday Discuss. R. Soc.* **1992**, *94*, 199.
(193) Mayne, A. J.; Avery, A. R.; Knall, J.; Jones, T. S.; Briggs, G. A. D.; Weinberg, W. H. *Surf. Sci.* **1993**, *284*, 247.
(194) Takayanagi, K.; Tanishiro, Y.; Takahashi, M.; Takahashi, S. *J. Vac. Sci. Technol. A* **1985**, *3*, 1502.
(195) Hamers, R. J.; Tromp, R. M.; Demuth, J. E. *Phys. Rev. Lett.* **1986**, *56*, 1972.
(196) Sakurai, T.; Hasegawa, Y.; Hashizume, T.; Kamiya, I.; Ide, T.; Sumita, I.; Pickering, H. W.; Hyodo, S. *J. Vac. Sci. Technol. A* **1990**, *8*, 259.
(197) Mortensen, K.; Chen, D. M.; Bedrossian, P. J.; Golovchenko, J. A.; Besenbacher, F. *Phys. Rev. B* **1991**, *43*, 1816.
(198) Boland, J. J. *Surf. Sci.* **1991**, *244*, 1.
(199) Boland, J. J. *J. Vac. Sci. Technol. B* **1991**, *9*, 764.
(200) Froitzheim, H.; Kohler, U.; Lammering, H. *Surf. Sci.* **1985**, *149*, 537.
(201) Greenlief, C. M.; Gates, S. M.; Holbert, P. A. *Chem. Phys. Lett.* **1989**, *159*, 202.
(202) Greenlief, C. M.; Gates, S. M.; Holbert, P. A. *J. Vac. Sci. Technol. A* **1989**, *7*, 1845.
(203) Olander, D. R.; Balooch, M.; Abrefah, J.; Siekhaus, W. J. *J. Vac. Sci. Technol. B* **1987**, *5*, 1404.
(204) Memmert, U.; Berko, A.; Behm, R. J. *Surf. Sci.* **1995**, *325*, L441.
(205) Leibsle, F. M.; Samsavar, A.; Chiang, T. C. *Phys. Rev. B* **1988**, *38*, 5780.
(206) Pelz, J. P.; Koch, R. H. *J. Vac. Sci. Technol. B* **1991**, *9*, 775.
(207) Pelz, J. P. *Phys. Rev. B* **1990**, *42*, 3761.
(208) Lyo, I. W.; Avouris, P.; Schubert, B.; Hoffmann, R. *J. Phys. Chem.* **1990**, *94*, 4400.
(209) Wintterlin, J.; Avouris, P. *Surf. Sci. Lett.* **1993**, *286*, L529.
(210) Wintterlin, J.; Avouris, P. *J. Chem. Phys.* **1994**, *100*, 687.
(211) Boland, J. J.; Villarrubia, J. S. *Science* **1990**, *248*, 838.
(212) Boland, J. J.; Villarrubia, J. S. *Phys. Rev. B: Condens. Matter* **1990**, *41*, 9865.
(213) Schnell, R. D.; Rieger, D.; Bogen, A.; Wandelt, K.; Steinmann, W. *Solid State Commun.* **1985**, *53*, 205.
(214) Feltz, A.; Memmert, U.; Behm, R. J. *Surf. Sci.* **1994**, *307−309*, 216.
(215) Lander, J. J. *Surf. Sci.* **1964**, *1*, 125.
(216) Telieps, W.; Bauer, E. *Surf. Sci.* **1985**, *162*, 163.
(217) Martel, R.; Avouris, P. *Science* **1996**, submitted.
(218) Feltz, A.; U, M.; Behm, R. J. *Chem. Phys. Lett.* **1992**, *192*, 271.
(219) Seiple, J.; Pecquet, J.; Meng, Z.; Pelz, J. P. *J. Vac. Sci. Technol. A* **1993**, *11*, 1649.
(220) Avouris, P. *J. Phys. Chem.* **1990**, *94*, 2246.
(221) Avouris, P.; Wolkow, R. *Phys. Rev. B* **1989**, *39*, 5091.
(222) Wolkow, R.; Avouris, P. *Phys. Rev. Lett.* **1988**, *60*, 1049.
(223) Tanaka, S.; Onchi, M.; Nishijima, M. *Surf. Sci.* **1987**, *191*, L756.
(224) Kubler, L.; Hlil, E. K.; Bolmont, D.; Gewinner, G. *Surf. Sci.* **1987**, *183*, 503.
(225) Bozso, F.; Avouris, P. *Phys. Rev. B* **1988**, *38*, 3943.
(226) Hirayama, H.; Koyama, K.; Hiroi, M.; Tatsumi, T. *Appl. Phys. Lett.* **1990**, *57*, 780.
(227) Lyo, I.-W.; Kaxiras, E.; Avouris, P. *Phys. Rev. Lett.* **1989**, *63*, 1261.
(228) Avouris, P.; Lyo, I. W.; Bozso, F.; Kaxiras, E. *J. Vac. Sci. Technol. A* **1990**, *8*, 3406.
(229) Chen, P. J.; Colaianni, M. L.; Yates, J. T., Jr. *J. Appl. Phys.* **1992**, *72*, 3155.
(230) Bedrossian, P.; Meade, R. D.; Mortensen, K.; Chen, D. M.; Golovchenko, J. A. *Phys. Rev. Lett.* **1989**, *63*, 1257.
(231) Bedrossian, P.; Mortensen, K.; Chen, D. M.; Golovchenko, J. A. *Nucl. Instrum. Methods Phys. Res.* **1990**, *B48*, 296.
(232) Headrick, R. L.; Robinson, I. K.; Vlieg, E.; Feldman, L. C. *Phys. Rev. Lett.* **1989**, *63*, 1253.
(233) Yoshinobu, J.; Fukushi, D.; Uda, M.; Nomura, E.; Aono, M. *Phys. Rev. B* **1992**, *46*, 9520.
(234) Yoshinobu, J.; Tsuda, H.; Onchi, M.; Nishijima, M. *Chem. Phys. Lett.* **1986**, *30*, 170.
(235) Chu, S.-Y.; Anderson, A. B. *Surf. Sci.* **1988**, *194*, 55.
(236) Weiner, B.; Carmer, C. S.; Frenklach, M. *Phys. Rev. B* **1991**, *43*, 1678.
(237) Wang, Y.; Shan, J.; Hamers, R. J. *J. Phys. Chem.* **1996**, submitted for publication.
(238) Wang, Y.; Hamers, R. J. submitted for publication, 1996.

CR950213K